

## COMPACT CORE GALAXIES IN THE RESOLVE SURVEY

ELAINE M. SNYDER<sup>1</sup>, SHEILA J. KANNAPPAN<sup>1</sup>, DARA J. NORMAN<sup>2</sup>, ASHLEY S. BITTNER<sup>1</sup>, MARK A. NORRIS<sup>3</sup>, KATHLEEN D. ECKERT<sup>1</sup>, IAN DELL'ANTONIO<sup>4</sup>, CALLIE HOOD<sup>1</sup>, SAMANTHA DALLAS<sup>4</sup>, DAVID V. STARK<sup>1</sup>, AMANDA J. MOFFETT<sup>1,5</sup>, AND THE RESOLVE TEAM

<sup>1</sup>Department of Physics and Astronomy, University of North Carolina, 141 Chapman Hall CB 3255, Chapel Hill, NC 27599, USA; emsnyder@live.unc.edu

<sup>2</sup>National Optical Astronomical Observatory, 950 N Cherry Ave, Tucson, AZ 85719, USA

<sup>3</sup>Jeremiah Horrocks Institute, University of Central Lancashire, Preston, PR1 2HE, United Kingdom

<sup>4</sup>Department of Physics, Brown University, Box 1843, 182 Hope Street, Barus & Holley, Providence, RI 02912 and

<sup>5</sup>International Centre for Radio Astronomy Research (ICRAR), The University of Western Australia, 35 Stirling High-way, Crawley, WA 6009, Australia

*Draft version May 18, 2016*

### ABSTRACT

We analyze the complete set of 96 “compact core galaxies” (CCGs) in the volume-limited RESOLVE survey to investigate their formation and evolution in relation to compact galaxies such as ultra compact dwarfs (UCDs), compact ellipticals (cEs), and dwarf ellipticals (dEs) across a broad statistical distribution of environments. To identify CCGs, we use GALFIT to perform one-component Sérsic fits for all galaxies in RESOLVE with UKIDSS *Y*-band imaging (98% of the survey), which produces seeing-deconvolved effective radius ( $R_{\text{eff}}$ ) measurements. Candidate CCGs are selected to have  $R_{\text{eff}} < 1000$  pc. Two component (core and envelope) Sérsic fits are then performed on the candidates with Sérsic  $n$  fixed at 1 for an exponential disk profile for the envelope. We finalize the CCG sample by selecting core  $R_{\text{eff}} < 800$  pc, an upper limit that encompasses all of the similarly compact stellar systems (UCDs, cEs) included in the Archive of Intermediate Mass Stellar Systems (AIMSS) catalog. We quantify the morphologies of CCGs by taking the logarithm of the ratio of the light in each component. The result is a smooth continuum of CCGs that range from envelope-dominated to core+envelope to core-dominated, which may represent earlier or later evolutionary stages of CCGs. With GALEX *NUV*, SDSS *ugriz*, and 2MASS/UKIDSS *YJHK* data, we derive colors and star formation histories and find that a significant number of CCGs live on the blue sequence and have recently formed stars. We find that CCGs naturally occur in a range of environments from free floating to cluster. We derive velocity dispersions ( $\sigma$ ) for eight CCGs from Gemini IFU data and SOAR spectroscopy. Comparing to other RESOLVE galaxies and AIMSS cEs/dEs, we search for CCGs offset to higher or lower dispersion in the dispersion-stellar mass relation, which may indicate tidal stripping (as expected for cEs) or dissipative formation (as expected for dEs), respectively. We classify CCGs as CSS-like (small radius and high dispersion), dE-like (large radius and low dispersion), or crossover (small radius and low dispersion). Initial results show four CCGs are dE-like and four are crossovers.

*Keywords:* galaxies: formation, evolution — surveys

### 1. INTRODUCTION

The term compact stellar system (CSS) encompasses a class of galaxies that spans the radius range between globular clusters (GCs) and normal elliptical galaxies (Es). Different types of CSSs include compact elliptical galaxies (cEs; Faber 1973) and ultra compact dwarf galaxies (UCDs; Phillips et al. 2001). There are many unanswered questions about how CSSs form and evolve through time. One fact that makes the study of these compact galaxies so intriguing is their apparent scarcity, which raises the question as to whether they are an intermediate and short-lived evolutionary phase in the life of a galaxy, or simply hard to find due to their size. Only in the last 15 years have we discovered enough ( $\sim 40$ ) of these objects to enable studies of their formation scenarios.

CSSs have half-light radii ( $R_{\text{eff}}$ ) typically ranging from  $\sim 10$ –600 pc (e.g., Norris et al. 2014), and there are multiple theories for how they form. The smaller of the CSSs, UCDs may simply be the high mass extension of the GC population (Drinkwater et al. 2000; Mieske et al. 2002). There is also evidence that UCDs are created via the tidal stripping of nucleated dwarf galaxies (Bekki et al. 2001; Bekki & Freeman 2003; Norris & Kannappan 2011; Jennings et al. 2015; Zhang et al. 2015). Seth et al. (2014) find a supermassive black hole at the center of another UCD, providing further ev-

idence of tidal stripping being common for UCDs. Similarly, cEs are thought to be the result of tidal stripping events, as argued for the prototypical cE, M32 (Choi et al. 2002; Graham 2002; Huxor et al. 2011). More evidence is provided by the discovery of tidal streams near cEs (Smith Castelli et al. 2008; Chilingarian et al. 2009) and one cE, studied in Kormendy et al. (1997), that is believed to host a central massive black hole. On the other hand, Wirth & Gallagher, J. S. (1984), Kormendy et al. (2009), and Kormendy & Bender (2012) argue that cEs are the low mass extension to the normal E population created via dissipative formation in gas rich environments, such as during mergers or the two-phase formation process detailed in Oser et al. (2010). One of the most successful recent searches for CSSs is the AIMSS catalog (Norris et al. 2014): with many newly discovered UCDs and cEs to examine, the authors argue that all of the above scenarios for UCD and cE formation occur.

In contrast to CSSs, dwarf elliptical galaxies (dEs; Sandage et al. 1985) and their nucleated counterparts (dE,Ns; Binggeli et al. 1984) are quite common, especially in clusters where they were first discovered. In fact, Binggeli & Cameron (1991) find that of 225 galaxies present in the center of Virgo cluster, 174 are classified as dEs or dE,Ns based on their surface brightness profiles. While dEs are typically larger than

CSSs with  $R_{\text{eff}}$  ranging from  $\sim 600$  pc up to  $\sim 2000$  pc (e.g., Norris et al. 2014), the cores of dE,Ns are comparable in size to CSSs and reside within larger envelopes that are dE-sized. Similar to cEs, dEs are often thought to be either tidally stripped remnants (Crnojević et al. 2014) or the low mass extension to elliptical galaxies (Kormendy & Bender 2012). They could also be the remnants of late-type disk galaxies or luminous blue compact dwarfs that were ram-pressure stripped and quenched as they entered the cluster environment (Lisker et al. 2013; Crawford et al. 2016). There is also evidence that dE,Ns become UCDs as they fall deeper into the cluster core and are further stripped (Pfeffer & Baumgardt 2013; Zhang et al. 2015; Liu et al. 2015).

Given the similarities in formation scenarios between CSSs and dEs, we introduce the term “compact core galaxy” or “CCG” to encompass CSSs and dEs with core  $R_{\text{eff}}$  up to 800 pc. The goal of this paper is to study these galaxies as part of a continuum of compact galaxies in order to differentiate between formation scenarios. Clues to how CCGs form may be given by their environments, morphology (i.e. one- or two-component structure), star formation histories, and kinematics. We highlight these data below.

**Environments.** CSSs have been found in a large range of environments thus far. UCDs were first discovered in the Fornax cluster (Hilker et al. 1999; Drinkwater et al. 2000) and have since been found in the cores of several other clusters (Price et al. 2009; Madrid et al. 2010; Jones et al. 2006; Mieske et al. 2009; Misgeld et al. 2008), in groups (Evstigneeva et al. 2007), and near field galaxies (Hau et al. 2009; Norris & Kannappan 2011). M32 was first discovered in our Local Group (Faber 1973) near M31, and more cEs were later found in clusters (Chilingarian et al. 2007; Smith Castelli et al. 2012; Price et al. 2009) and other groups (Huxor et al. 2011; Chilingarian & Bergond 2010). As stated previously, dEs and dE,Ns are common in clusters (Smith Castelli et al. 2012; Koo et al. 1994; Guzmán et al. 1996; Crawford et al. 2016), but have also been found near groups (Crnojević et al. 2014; Penny et al. 2014). Only cEs have been found “free floating”, meaning there is no host galaxy at all: Huxor et al. (2013) and Paudel et al. (2014) both find one cE separated from other galaxies by  $\sim 840$  and  $\sim 600$  kpc, respectively.

Environment affects formation scenarios in different ways. One possibility is that CSSs found in group or cluster environments may be tidally stripped remnants, whereas free floating CSSs may rather be dissipatively formed like Es. However, Chilingarian & Zolotukhin (2015) argue that these free-floating cEs could actually be tidally-stripped cores that are ejected from groups and clusters during the tidal stripping process. The recent discovery of a free-floating GC and UCD that have likely been tidally stripped supports this idea (Sandoval et al. 2015).

**Morphologies.** CSSs have been found to exhibit either one component (i.e., just a core) or two component (i.e., a core plus a surrounding envelope of gas and stars) morphology. Graham (2002) has shown that M32’s light profile is best fit with a core plus a surrounding exponential disk profile, which points toward a tidal-stripping origin. Pfeffer & Baumgardt (2013) use N-body simulations to predict that UCDs that are tidally stripped remnants will also display multi-component surface brightness profiles due to lingering outer galaxy structures. Conversely, dissipative processes such as the two-phase formation scenario proposed by Oser et al. (2010) cause cores to form as gas rushes to the center during mergers or the convergence of streams of cold gas. This core is then “puffed

up” through time as it interacts with other galaxies. The free-floating cE discovered in Huxor et al. (2013), shown to have only a one-component light profile, may be an example of the first step in this two-phase formation. It is important to note that these effects may vary based on the degree of stripping and the time passed since the stripping or dissipative formation occurred.

By their nomenclature, dEs and dE,Ns have already been divided into one and two component morphologies. Studies have found that dE,Ns are usually more common than dEs: Grant et al. (2005) find that the majority of Virgo cluster dwarfs are indeed nucleated and speculate that at least some of the nuclei were formed out of an existing non-nucleated galaxy from infalling gas. Another possibility is that the morphology is already in place as dEs/dE,Ns form. For example, Mastropietro et al. (2005) use N-body simulations to show that as the progenitors of dEs/dE,Ns enter clusters, their morphologies are greatly disrupted but disks may not be completely destroyed by ram pressure or tidal stripping, leaving the dEs/dE,Ns we observe today.

**Star formation histories.** Colors and star formation rates are useful since they may point to recent star formation as a part of tidal stripping or dissipative formation. The typical thought is that CSSs are “red and dead”, and some studies even cut on color when selecting CSS samples (Chilingarian & Zolotukhin 2015). Drinkwater et al. (2000) have examined the stellar populations of CSSs and find that CSSs are usually best fit as having older stellar populations. However, Norris & Kannappan (2011) find a UCD with young stellar populations and smoking gun signs of tidal stripping origins, including counter-rotating gas and a short dynamical friction timescale. Maraston et al. (2004) also find a young tidally formed UCD near the merger remnant galaxy NGC 7252. This evidence makes it clear that CCSs can have young and old stellar populations.

For dEs and dE,Ns, there is similar diversity in color. Smith Castelli et al. (2012) find dEs in the Antlia cluster with both red and blue colors. Drinkwater et al. (2000) and Ferrarese et al. (2006) study the colors of dE,Ns and find that the cores of dE,Ns tend to have younger stellar populations compared to their host galaxies. Grant et al. (2005) also find that two-fifths of the Virgo dE,Ns have young cores compared to their envelopes, while three-fifths display the opposite trend.

**Kinematics.** The last useful tool we have for discerning between formation scenarios is the galaxy’s stellar velocity dispersion ( $\sigma$ ). Bender et al. (1992) and Bekki & Freeman (2003) show that  $\sigma$  will remain largely unchanged when tidal stripping occurs, even though the  $R_{\text{eff}}$  and stellar mass will be greatly reduced. Thus, galaxies that are offset to higher  $\sigma$  in a Faber-Jackson (stellar mass –  $\sigma$ ) relation (Faber & Jackson 1976) are most likely tidally stripped, while galaxies falling along the relation are most likely the low-mass extension of normal Es. Lending evidence to this idea are the tidally-stripped UCD found in Maraston et al. (2004) and the prototypical cE, M32, both of which have much larger velocity dispersions than expected for their mass.

In this paper, we present a complete sample of CCGs derived from the volume-limited RESOLVE survey, along with key data quantifying their morphologies, environments, star formation histories, and kinematics. We use this sample to examine the formation scenarios and evolution of CSSs and dEs/dE,Ns simultaneously as a spectrum of compact galaxies that span the gap from GCs to Es. Because we have derived a complete sample from RESOLVE, our sample contains CCGs

at every evolutionary stage. This paper is organized as follows. We describe our parent sample, the RESOLVE survey, in § 2.1 and our comparison sample, the AIMSS catalog, in § 2.2. Our methods for performing seeing-deconvolved one and two component fits for the entire RESOLVE sample using GALFIT are presented in § 2.3.1. We detail the selection of the CCG sample from the RESOLVE survey and quantify our CCG demographics in § 2.3.2. We describe our photometric, environmental, and spectroscopic data and analysis in § 3. We present a statistical distribution of environments, star formation histories, and velocity dispersions for the complete sample in § 4. In § 5, we present a discussion of our results in the context of CCG formation and evolution. Lastly, the summary and future work are given in § 6.

## 2. SAMPLES

### 2.1. The RESOLVE survey

We use the RESOLVE survey (Kannappan et al. 2008, Kannappan et al., in prep) as the parent sample for our census of CCGs. RESOLVE is ideal because it is an unusually complete and volume-limited survey, which allows us to find CCGs at all evolutionary stages. RESOLVE falls within the footprint of the Sloan Digital Sky Survey (SDSS, York et al. 2000), and covers equatorial strips in both semesters: A for the northern spring sky and B for the northern fall sky, which overlaps much of Stripe-82. With  $H_0 = 70 \text{ km s}^{-1}$ , RESOLVE-A spans  $\sim 38,400 \text{ Mpc}^3$  and occupies the region  $131.25^\circ < \text{RA} < 236.25^\circ$  and  $0^\circ < \text{Dec} < 5^\circ$ , while RESOLVE-B spans  $\sim 13,700 \text{ Mpc}^3$  and occupies the region  $330^\circ < \text{RA} < 45^\circ$  and  $-1.25^\circ < \text{Dec} < 1.25^\circ$ . Both semesters cover the redshift range  $4500 \text{ km s}^{-1} < cz < 7000 \text{ km s}^{-1}$ .

RESOLVE’s exceptional completeness is obtained by making use of multiple redshift surveys to recover galaxies that were missed in SDSS due to (i) fiber collisions, (ii) the “shredding” of galaxies in which the pipeline breaks up a single galaxy into individual pieces so no one piece meets the magnitude cut, and (iii) the intentional exclusion of low surface brightness galaxies ( $\mu_{50} < 24.5 \text{ mag arcsec}^{-2}$ ), even if they meet the magnitude cut. We supplement the SDSS main redshift survey with additional redshifts from archival sources, including the Updated Zwicky Catalog (Falco et al. 1999), HyperLeda (Paturel et al. 2003), 6dF (Jones et al. 2009), 2dF (Colless et al. 2001), GAMA (Driver et al. 2011), and ALFALFA (Haynes et al. 2011), to achieve  $\sim 12\%$  higher completeness in RESOLVE-A and  $\sim 25\%$  higher completeness in RESOLVE-B (Eckert et al. 2015).

With its improved redshift recovery, RESOLVE is complete down to absolute  $r$ -band magnitudes of  $-17.33$  and  $-17.0$  for the A and B semesters, respectively. To derive the stellar mass completeness limits of RESOLVE, Eckert et al. (2016) use the known stellar masses and magnitudes of all RESOLVE galaxies to determine the stellar mass limit above which no more than 2% of objects have an  $r$ -band magnitude fainter than the stated magnitude completeness limit. These values are  $M_* \sim 10^{8.9} M_\odot$  for the A semester and  $M_* \sim 10^{8.7} M_\odot$  in the B semester (Figure 8 in Eckert et al. 2016). These stellar mass completeness limits allow us to reach down to CSSs with sizes and masses similar to cEs (see § 4.1 for more details), but restricts us from reaching down to UCD masses.

An important caveat to RESOLVE’s completeness is that the survey is preferentially incomplete for the very objects this study is focused on, cEs. Such round objects can often

be mistaken for stars in redshift surveys using tools such as the `class_star` parameter in Source Extractor (Bertin & Arnouts 1996). We are engaged in ongoing efforts to use photo-z estimates to recover some of these objects.

### 2.2. The AIMSS catalog

We use the Archive of Intermediate Mass Stellar Systems (AIMSS) catalog (Norris et al. 2014; Forbes et al. 2014; Janz et al. 2015) as a reference sample for our CCGs. AIMSS is a catalog of spectroscopically confirmed CSSs found near field galaxies, in groups, and in clusters, and includes both previously known and newly discovered objects. The AIMSS CSS discovery process was as follows. First, a search was conducted in the HyperLeda redshift catalog (Paturel et al. 2003) for all galaxies with  $M_B < -15$  and distances between  $\sim 7$  and 200 Mpc (close enough to ensure any CSSs with  $R_{\text{eff}} > 50$  pc would be resolved in any available HST imaging). The team then searched the Hubble Space Telescope archive for WFC2, ACS, and WFC3 imaging within 150 kpc in projection of the selected galaxies. Next, Source Extractor was run on the HST images, and candidates were identified using a training set of previously known CSSs from the literature. After vetting by eye and cross-matching to ensure none are previously known, spectra were obtained for redshift confirmation and measurements of velocity dispersions. AIMSS also includes literature data for previously known UCDs, cEs, dEs, dE,Ns, dwarf spheroidals, dwarf S0s, young massive clusters, and Es. The catalog provides a compilation of absolute  $V$ -band magnitude, stellar mass, half-light radius, and velocity dispersion for each of its objects. Thus, though not a statistically-defined sample, AIMSS provides a useful reference catalog to which we can compare our CCGs. We also note that the objects in AIMSS are not decomposed, meaning their  $R_{\text{eff}}$  are all single component fits. We discuss this more in § 5.

## 2.3. CCG sample selection

### 2.3.1. Deconvolution of RESOLVE galaxies

We begin our analysis by deriving seeing-deconvolved  $R_{\text{eff}}$  measurements for all galaxies in the RESOLVE sample. For this task we employ GALFIT (Peng et al. 2002) to deconvolve the seeing point spread function (PSF) and to perform one and two component fits to each galaxy. Deconvolution is especially important since the smallest galaxies in RESOLVE are most affected by seeing, and accurate radius measurements are crucial for the study of these objects.

GALFIT needs the following input files to function properly: an initial input file, an image of the galaxy, a PSF image, an image mask, and a constraint file. We obtain or construct these items as follows:

**The initial input file:** The initial input file gives GALFIT the file paths to the image, PSF, mask, and constraint file, and also holds the initial guesses for our fit parameters. For the one component fits, we set up our input file to include a section to measure the level of the sky background and another section to fit a Sérsic profile (Sérsic 1963, 1968) to the galaxy. The Sérsic model will find a best fit for the following parameters: central x & y position of the model, integrated magnitude,  $R_{\text{eff}}$ , Sérsic n, axial ratio (b/a), and position angle. We use initial values for the magnitude,  $R_{\text{eff}}$ , b/a, and PA that are derived from RESOLVE’s custom processed photometric data (see § 3.1 for more details).

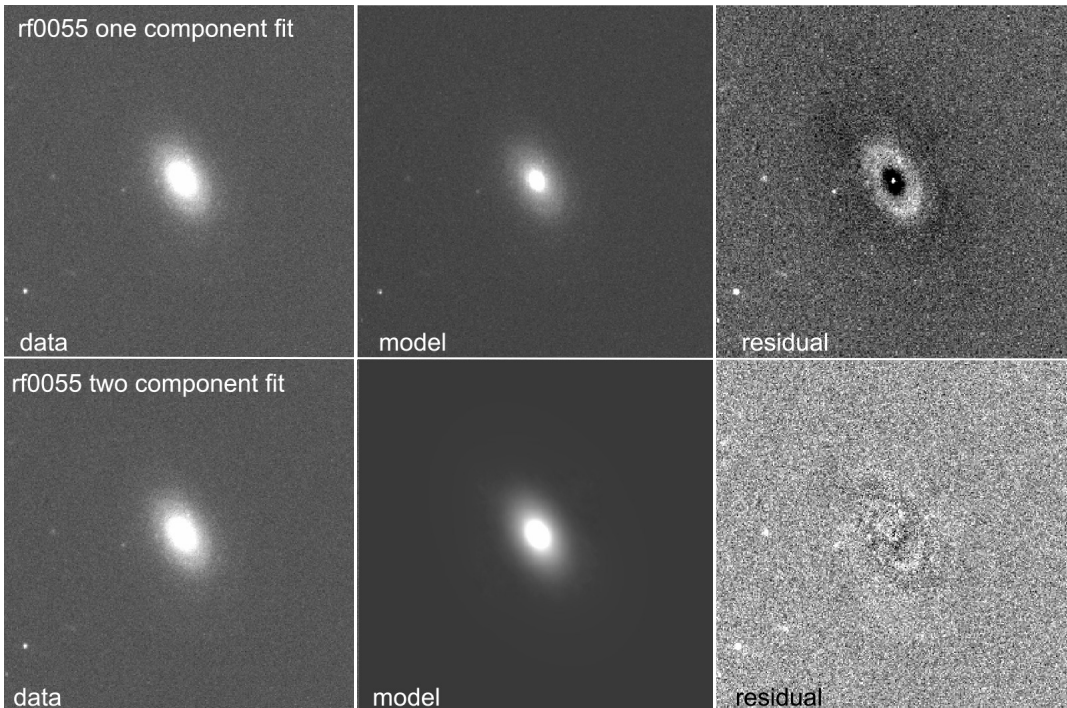


**Figure 1.** Model inputs and outputs from GALFIT. The left column shows the UKIDSS  $Y$ -band image cutout around the galaxy. The middle column shows the best fit GALFIT model, and the right column shows the residuals (data-model). The top row shows the one component fit for the RESOLVE galaxy, rf0055. As seen in the residual image, the model is overfitting the inner bulge, and underfitting the outer envelope. The bottom row shows the two component fit for the same galaxy. We are now able to fit both the inner bulge and the outer envelope. The residual is much cleaner, although there may be some spiral structure remaining.

**Imaging data:** We use publicly-available high resolution  $Y$ -band imaging from the UKIDSS Large Area Survey (Lawrence et al. 2007). This data set was chosen because it covers both RESOLVE-A and RESOLVE-B and offers  $\sim 0.8''$  seeing resolution corresponding to  $\sim 350$ pc at RESOLVE distances in turn letting us span down to the sizes of cE-like galaxies. The  $Y$  band is advantageous too, since it probes the underlying stellar population and will not skew our measurements to larger radii if the galaxy is currently experiencing a starburst. We download  $\sim 10' \times 10'$  images of each galaxy from the WFCAM Science Archive<sup>1</sup>. While GALFIT does not require images this large to operate normally, we choose this size so that there will be more stars in the field of view which is useful when constructing the PSF image. There are 25 galaxies in RESOLVE (2% of the survey) that do not have UKIDSS imaging and thus are excluded from our analysis.

**The PSF image:** GALFIT uses the PSF image to deconvolve the galaxy light profile from the seeing, thereby removing the effects of atmospheric scattering of the galaxy light as the data was taken. We build our PSF image via the following steps:

1. We begin by running Source Extractor on the image to identify every object in the frame, including stars, galaxies, and even sometimes hot pixels. Source Extractor outputs a text file that has estimates of each object's flux, elongation, ellipticity, radius, and `class_star`.
2. With this information, we select stars to use for building our PSF. The limiting parameters are (1) that the flux must be between 5,000 – 100,000 counts to ensure no extremely faint or saturated stars are included, (2) that the ellipticity be less than 0.2 to ensure we are selecting round objects, (3) that the effective radius of the star be greater than 1 pixel to avoid selecting hot pixels, and (4) that `class_star` is greater than 0.6 to ensure the objects we're picking are most likely stars. We also make sure the stars are not near the image edges, since there can sometimes be image artifacts there. Lastly, we make sure to not include the galaxy we are going to fit, since the cE-like galaxies can sometimes appear to be stars.
3. We next make  $101 \times 101$  pixel cutouts of each object detected, with the flux peak at pixel  $x = 51, y = 51$ .
4. Background subtraction is then performed by taking the median of the entire cutout and then subtracting each pixel by this median value.
5. We then reject any of the cutouts that have a background median value greater than  $2\sigma$  from the mean of the background median values for every cutout. This ensures we are not including any cutouts that have stars with large or bright neighboring objects. We are now left with background-subtracted cutouts of stars with no neighbors that could affect our stacking.

<sup>1</sup> [was.roe.ac.uk/](http://was.roe.ac.uk/)

6. Before we can combine all the cutouts, we must normalize the flux of each central star to the same amplitude. To do this, we run each cutout through Source Extractor once more to obtain the fluxes of each central star and use these to weight the cutouts accordingly. We calculate the weight for each cutout as follows: (1) we find the central star with the highest flux of all the cutouts and then (2) divide every flux by this maximum flux. We then divide each cutout by its corresponding weight, which makes each central star have the same amplitude.
7. We then take the median of all the weighted cutouts to create a semi-complete PSF.
8. Lastly, we normalize the semi-complete PSF from Step 7 by dividing each pixel in the frame by the total flux in the image. We find the total image flux by taking the mean of each pixel and multiplying that by the number of pixels in the image (so,  $101 \times 101$ ). This ensures that the final PSF image is normalized, i.e., the sum of the flux in each pixel of the cutout would equal one.

Our last step is to fit a 2D Gaussian to the PSF to determine a rough estimate seeing full width half max (FWHM), as a sanity check. We find that the average FWHM for all PSFs is  $\sim 0.9''$ , only slightly worse than the  $\sim 0.8''$  seeing expected for UKIDSS imaging.

**The mask image:** GALFIT uses the mask image to ignore any objects neighboring our galaxy while it is completing the fit. The first step in making the mask is to create an image that has the same dimensions as our input image but with each pixel value equaling zero. We again use Source Extractor to compile a list of all the objects in the input image, and use this list to replace the pixel values at the coordinates of the located objects with one.

**The constant file:** The constraint file hosts the limits we are willing to accept for each of the fit parameters. The constraints for x & y position in the image, integrated magnitude,  $R_{\text{eff}}$ , Sérsic n, axial ratio (b/a), and position angle for the one component fits are listed in Table 1. We change the constraint file for the two component fits later in the analysis.

parameter	constraint
x & y position	$\pm 5$ pixels from input value
integrated magnitude	0 – 40
$R_{\text{eff}}$	0.2 – 750 pixels
Sérsic n	0.1 – 8
axial ratio (b/a)	0 – 1
position angle (PA)	-360 – 360

**Table 1**  
Summary of the constraints imposed on our GALFIT models for our initial one component fits for the entire RESOLVE sample.

We use all of the above to obtain a one component, seeing-deconvolved fit for every galaxy in the RESOLVE survey. We then perform the two component fits as follows. We use the

output of the one component fit as the basis of the input file for the two component fit. The first two sections in the two component fit initial input file will be identical to the output of the one component fit. We then add a third section to include a second Sérsic fit, and change the initial guess for  $R_{\text{eff}}$  to be double that of the one component best fit. This gives GALFIT a preliminary guess for the radius of an envelope. The PSF, image, and mask image will all be the same as before. We add to the constraint file the same constraints as listed in Table 1, but for the third section. In other words, there will be two sets of constraints in the file now, with the first set applying to the first Sérsic fit and the second set applying the second Sérsic fit. The constraints for each parameter are the same for both sets. We do not further constrain the two component fits since we are looking for general fits to the wide variety of galaxies in RESOLVE and do not want to over-constrain the fits.

For both the one and two component fits, GALFIT outputs the best fits for central x & y position of the model, integrated magnitude,  $R_{\text{eff}}$ , Sérsic n, axial ratio (b/a), and position angle as well as the  $\chi^2$ ,  $\chi^2/\nu$  and number of degrees of freedom for the fit. Also output is a fits file that contains the data, best fit model, and residual images. See Figure 1 for example one and two component fits for the RESOLVE galaxy rf0055.

### 2.3.2. Selection of CCGs

Now that we have seeing-deconvolved  $R_{\text{eff}}$  values for the entire RESOLVE sample, we begin our search for compact core galaxies. We select a maximum cutoff core-only radius for CCGs at 800 pc. Comparing to the CSSs and dEs/dE,Ns in the AIMSS catalog, this upper limit ensures that we are selecting CSSs in RESOLVE with  $R_{\text{eff}}$  up to 600 pc and lets us include the smallest dEs and dE,Ns as well.

We start by using the one component fit from the above analysis and select galaxies with  $R_{\text{eff}}$  values  $< 1000$  pc. Since we are looking for galaxies with compact cores, extending to  $R_{\text{eff}} \sim 1000$  pc allows us to select objects with cores that are dominating the light and therefore may have a smaller core  $R_{\text{eff}}$  in a two component fit. We do note that this limit is arbitrary, and it will be relaxed in the future to allow CCGs with larger envelopes be included in the sample (see § 6). We also limit the  $\chi^2/\nu$  to be  $< 1.3$ , since values above this represent galaxies with large residuals, which are normally spiral or irregular galaxies. After this selection, we are left with 124 galaxies in the CCG candidate sample.

Next, we perform new two component fits using different constraints: (1) the central x and y positions are taken from the one component fit and are held constant for both Sérsic components, (2) the  $R_{\text{eff}}$  of the second Sérsic component fit is constrained to always be larger than that of the first Sérsic component fit, and (3) the Sérsic n of the second component is held constant at 1 representing an exponentially decreasing disk profile. We let the values of  $R_{\text{eff}}$ , integrated magnitude, b/a ratio, and PA change for both fits. By doing this, we are forcing GALFIT to fit on a core (the first Sérsic component fit) and disky envelope (the second Sérsic component fit) for each CCG candidate.

We then examine the fits by eye and create our final CCG sample by selecting where the core  $R_{\text{eff}} < 800$  pc and  $\chi^2/\nu < 1.3$  to again exclude poor fits. Our sample is thus comprised of 96 CCGs in total (63 from RESOLVE-A and 33 from RESOLVE-B). This represents  $\sim 6\%$  of the total RESOLVE galaxy sample. Figure 4 shows their distribution in stellar mass and decomposed  $R_{\text{eff}}$  compared to other RE-

SOLVE galaxies and the AIMSS cEs and dEs. For the RESOLVE sample, we are plotting the one component fits, while for the CCGs, we are plotting the core  $R_{\text{eff}}$  from the fixed two component fits.

We quantify the amount of light in the core vs. the envelope by taking a ratio of the flux in each component. We compute the fluxes using  $m = -2.5 \times \log(\text{flux})$ , where  $m$  is the integrated magnitude output from GALFIT. GALFIT calculates the integrated magnitude for Sérsic profiles using the equations:

$$\text{flux} = 2 R_{\text{eff}}^2 \Sigma_e e^\kappa n (\kappa)^{-2n} \Gamma(2n) (b/a) / R(C_0; m) \quad (1)$$

$$\kappa \approx 1.999 n - 0.327 \quad (2)$$

$$m = -2.5 \log_{10}(\text{flux}/t_{\text{exp}}) + \text{mag}_\infty, \quad (3)$$

where  $\Sigma_e$  is the surface brightness at  $R_{\text{eff}}$ ,  $R(C_0; m)$  is a geometric correction factor when the azimuthal shape of the galaxy deviates from a perfect ellipse,  $t_{\text{exp}}$  is the exposure time of the image, and  $\text{mag}_\infty$  is the zero point magnitude of the image. Since GALFIT also outputs the Sérsic n values, we can also plot the one dimensional light profiles for each component. In Figure 2 we plot five CCGs spanning the range of  $\log(\text{flux ratio})$  values along with their one dimensional Sérsic light profiles. Since the fluxes are calculated using the two dimensional ellipsoidal shape of the galaxy, the one dimensional profile may not always match what we expect the  $\log(\text{flux ratio})$  value to be.

For each plot in this paper, we color code the CCGs by the logarithm of the flux ratio. CCGs with more light in the envelope will have  $\log(\text{flux ratio}) < 0$ , and will hereafter be called “envelope-dominated” CCGs. CCGs with more light in the core will have  $\log(\text{flux ratio}) > 0$ , and will hereafter be called “core-dominated” CCGs. CCGs with  $\log(\text{flux ratio}) \sim 0$  will have both a bright core plus an extended envelope, and will be called “core+envelope” CCGs.

We also note that there are some cases when GALFIT cannot find a core or an envelope, and will instead fit an extremely large and faint component instead. When this happens (11 out of 96 cases), we classify this fit as either all core/all envelope depending on which component was bad, i.e., assigning  $\log(\text{flux ratio}) = \text{minimum of all flux ratios } (-0.93)$  or  $\text{maximum of all flux ratios } (+1.31)$ <sup>2</sup>. In six of 96 cases, GALFIT fits identical  $R_{\text{eff}}$  values for both the first and second Sérsic components. We inspect their Sérsic plots by eye and see that these should be core-dominated CCGs. We assign these cases to have  $\log(\text{flux ratio}) = \text{maximum of all flux ratios } (+1.31)$  as well<sup>3</sup>.

## 3. METHODS

### 3.1. Photometry: galaxy colors, stellar and baryonic masses, and star formation rates

The RESOLVE survey overlaps with a number of photometric surveys, including GALEX NUV (Morrissey et al. 2007), SDSS-DR8 ugriz (Aihara et al. 2011), and UKIDSS YHK and/or 2MASS JHK (Skrutskie et al. 2006). These photometry data have been reprocessed to improve upon the standard SDSS data pipeline, as described in detail in Eckert et al. (2015). The main improvements in this processing are (1) improved sky subtraction following Blanton et al.

<sup>2</sup> An example of this case is CCG rf0250, which is plotted on the far right of Figure 2.

<sup>3</sup> An example of this case is CCG rf0003, which is plotted in the top right of Figure 9.

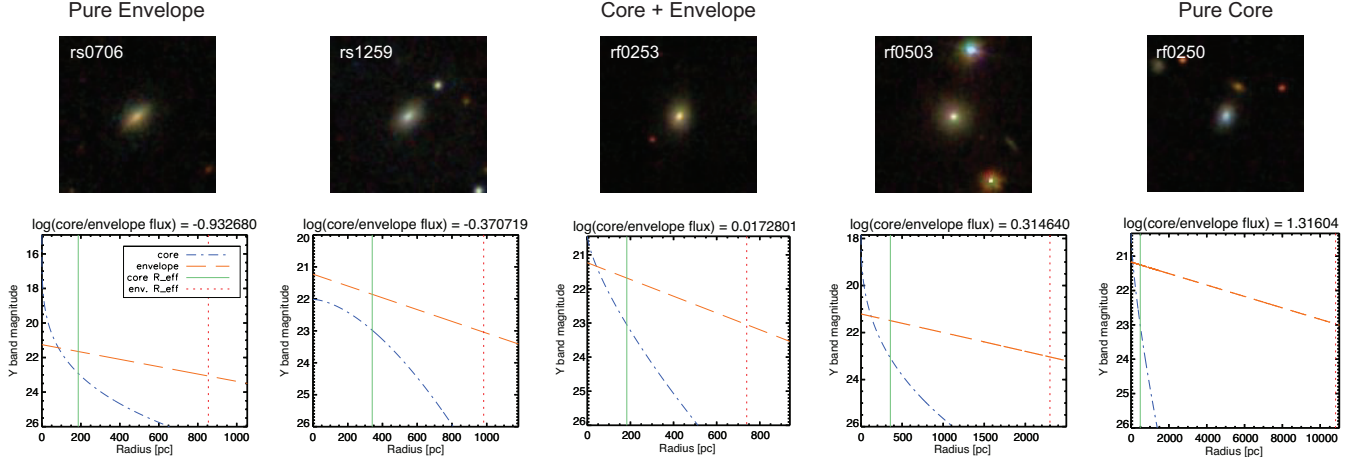


**Figure 2.** Five of the 96 CCGs in the final sample arranged in order from envelope-only to core+envelope to core-only from left to right. Images are taken from the SDSS-DR8 image list tool. The galaxy rf0250 is an example of one of eleven CCGs that was fit with a large diffuse envelope and has hence been reclassified as “core-dominated”.

(2011) for SDSS photometry plus custom background subtraction for UKIDSS/2MASS, (2) definition of elliptical apertures using the sum of the high S/N *gri* images to determine the PA and *b/a* ratio yielding improved sensitivity to the outer disk (if present), and (3) application of the same apertures to all bands, which allows us to measure magnitudes for galaxies that may not have been detected by automated survey pipelines, especially low surface brightness galaxies in 2MASS, UKIDSS, and GALEX. Then, total magnitudes are derived for each band using three methods to enable robust estimation of errors: an exponential outer disk fit, a curve of growth, and a color correction (Figure 2 in Eckert et al. 2015).

Stellar masses ( $M_*$ ), a long-term fractional stellar mass growth rate (FSMGR), and model colors are then derived from these reprocessed *NUVugrizYJHK* magnitudes using the spectral energy distribution (SED) modeling code described in Kannappan et al. (2013). We adopt the model grid from Kannappan et al. (2013) that combines old simple stellar populations with 2–12 Gyr age ranges and young stellar populations with either continuous star formation from 1015 Myr ago to 0–195 Myr ago, or with a simple stellar population with age either 360, 509, 641, 806, or 1015 Myr. A  $M_*$  likelihood distribution is calculated for each model, and the single value  $M_*$  is the median of the distribution. Kannappan et al. (2013) design their model to also estimate FSMGR, which is the ratio of stellar mass created in the last Gyr to the stellar mass previously existing (i.e., an FSMGR of 1 means that the galaxy has doubled its stellar mass in the last Gyr). Likelihood weighted model colors are also output with extinction corrections and *k*-corrections to  $z = 0$ .

Baryonic masses ( $M_{bary}$ ) are defined as  $M_* + M_{HI}$ . HI values for RESOLVE are from the blind 21cm ALFALFA survey (Haynes et al. 2011) and new pointed observations with the Greenbank and Arecibo telescopes (Stark et al., submitted). Eckert et al. (2016) calculates  $M_{bary}$  by performing pseudo-convolutions of the likelihood distribution for  $M_*$  as computed above with the likelihoods for  $M_{HI}$  computed in two ways. Galaxies with HI detections that are clean or successfully deconfused have Gaussian likelihood distributions with  $\mu = M_{HI}$  and  $\sigma$  = the systematic uncertainty of the measurement. For galaxies with weak upper limits, low S/N or severely confused detections, or no HI observations at all,

the log(gas-to-stellar mass) distributions from the photometric gas fraction calibration in Eckert et al. (2015) are used instead. For galaxies with strong upper limits, the likelihood in log(gas-to-stellar mass) is set to 1 at the upper limit value of log(gas-to-stellar mass). The single value  $M_{bary}$  is computed by taking the median of the resulting baryonic mass likelihood distribution for each galaxy.

### 3.2. Environment metrics

The volume-limited design of RESOLVE is advantageous to this study because it offers excellent environment information, allowing us to search for CCGs in all environments including groups, clusters, walls, and filaments. We explore the environments of CCGs using two different metrics: the mass of their group halo and their distance to a neighboring galaxy. The group halo mass allows us to look for CCG-host pairs that are M32–Andromeda analogues where tidal stripping is likely or conversely to look for CCGs in large groups where either ram-pressure or tidal stripping could be important. The distance to neighboring galaxies lets us examine if interaction may occur or look for analogs of the isolated galaxies found by Huxor et al. (2013) and Paudel et al. (2014).

Galaxy groups are identified using the friends-of-friends algorithm of Berlind et al. (2006) with linking lengths modified as described in Eckert et al. (2016), and the masses of the group halos are calculated based on the observed total *r*-band luminosity of galaxies in each group using abundance matching, as described in Blanton & Berlind (2007). More information on group identification can be found in Eckert et al. (2016). The nearest two-dimensional neighbor distances are computed using the RA and Dec coordinates for each galaxy along with a requirement that the neighbor be within  $\pm 500 \text{ km}^{-1}$  of the primary. Three-dimensional distances are also available based on Hubble’s Law distances, however the added errors that come with peculiar velocities make these values less reliable.

### 3.3. Kinematics

#### 3.3.1. SOAR spectroscopy

The RESOLVE survey gets the bulk of its spectroscopic data from the SOuthern Astrophysical Research (SOAR) Telescope, located at Cerro Tololo, Chile. We use the Good-

man Spectrograph (Clemens et al. 2004) along with RESOLVE’s custom-built image slicer with three parallel 1” slits to observe galaxies in either an emission- or absorption-line kinematic setup depending on whether the stellar continuum or gas emission lines are more prominent. With the absorption-line setup we are able to derive velocity dispersions, which are typically the best kinematic metric for CCGs. We use the highly-efficient 2100 l/mm VPH grating in order to cover a wavelength range 4858 – 5503Å, which includes stellar absorption lines such as H $\beta$ , the magnesium triplet, and Fe5270/5335. To achieve S/N  $\sim$  25 per Å, we bin each central spectrum to  $R_{\text{eff}}$ .

The reduction process is as follows: we use standard IRAF tasks to perform bias and overscan subtraction, trimming of the science data to remove unnecessary spatial coverage, and flat fielding. We then use LA\_COSMIC (van Dokkum 2001) to clean cosmic rays from each science exposure. We next complete a wavelength calibration and transformation. We lastly combine the individual exposures using the IRAF task *scombine*, leaving us with high signal-to-noise two-dimensional (y position vs. wavelength) spectra for each galaxy.

### 3.3.2. Gemini-South spectroscopy

A subset of the faintest or smallest galaxies in RESOLVE are observed with the Gemini-South IFU for their kinematics instead of SOAR. For this absorption-line setup, we use the B1200 grating in 1-slit mode to cover a spatial region of 3”  $\times$  5” and the spectral range 4200 – 5600Å. The B1200 grating offers 0.9Å resolution when binned spectrally by two. We calculate our exposure times such that we achieve S/N  $\sim$  25 per Å after binning by two pixels in the spectral direction and summing the fibers out to  $R_{\text{eff}}$ .

The spectral reduction proceeds as follows. Using the standard IRAF Gemini-GMOS data packages, we perform bias and overscan subtraction, spatial trimming, flat fielding and fiber identification. We next use the GMOS package gemCR-spec, a wrapper for LA\_COSMIC, to clean cosmic rays from each science exposure. We then correct the science frames for quantum efficiency differences between CCDs. Wavelength transformation, sky subtraction, and flux calibration are subsequently performed, and lastly, data cubes are made with 0.2” resolution (the width of each fiber). We stack the individual data cubes for each galaxy, leaving us with high S/N three-dimensional (x and y position vs. wavelength) spectra. We lastly create a World Coordinate System (WCS, Greisen & Calabretta 2002) solution for the data cube using the coordinates of the acquisition images and the position angle of the observation. More information on this process and the data reduction for the Gemini GMOS IFU in general can be found in the Appendix.

### 3.3.3. Velocity Dispersion Extraction

We use pPXF, the penalized pixel fitting code from Cappellari & Emsellem (2004) to measure the velocity dispersion ( $\sigma$ ) for each galaxy. This code fits a combination of high-resolution (FWHM = 0.55 Å) ELODIE-based model spectra from Maraston & Strömbäck (2011) to the observed input one dimensional spectrum, and determines a best fit solution for  $\sigma$ . To create a one dimensional spectrum from the SOAR spectra, we first do a gaussian fit in the y-direction of the image to find the central row, which represents the center of the galaxy. We then sum the spectra in each row above and below the central row out to the effective radius of the galaxy to create the one

dimensional spectrum. For the Gemini data cubes, we find the central position of the galaxy using its WCS solution, and then sum in all directions from the central spectrum out to the effective radius of the galaxy to create the one dimensional spectrum. Next, we must calculate the FWHM resolution of each spectrum so that pPXF can convolve the model spectra with the input spectrum before performing the fits. To do this, we measure the FWHM of three unblended emission lines in the comparison arc spectrum taken with our galaxy spectra during observations (for both SOAR and Gemini). The average of these three measurements is the resolution we feed pPXF. In Figure 3, we show an example of a pPXF fit for one of the CCGs observed with the Gemini-South IFU. In black is the observed spectrum that has been summed out to  $R_{\text{eff}}$  and in red is the pPXF best fit model spectrum, centered on the MgB triplet at  $\sim$  5275 Å.

A caveat to these fits is that they are not corrected for any stellar rotation, which will make absorption lines wider and thus skew the derived  $\sigma$  values toward higher values depending on the amount of rotation in each galaxy. Future work will include implementing a stellar rotation subtraction routine for these fits, but preliminary testing by binning the spectra to 1” instead of to  $R_{\text{eff}}$  shows little change between the derived  $\sigma$  values.

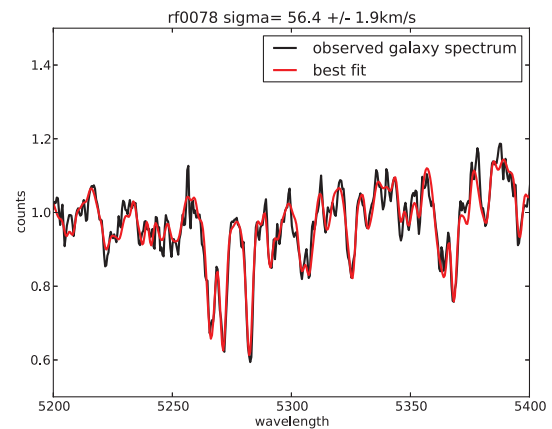


**Figure 3.** Summed Gemini-South IFU spectrum for the CCG rf0078. Overlotted in red is the pPXF best fit model spectrum. The spectrum is zoomed-in to show the MgB triplet fit at  $\sim$  5275 Å.

## 4. RESULTS

### 4.1. Morphologies

Figure 4 shows the deconvolved  $R_{\text{eff}}$  measurements for the entire RESOLVE sample, along with the CSSs and dEs of the AIMSS catalog. In grey are all RESOLVE galaxies, plotted using their one component fit  $R_{\text{eff}}$ . The CCG sample is plotted again with the core  $R_{\text{eff}}$  of the two component fits, causing them to shift down from the full RESOLVE sample. The symbol color for the CCGs represents the logarithm of the light ratio between the core and envelope, meaning that galaxies with log(flux ratio) near zero will have both a core and envelope, while galaxies with log(flux ratio) greater or less than zero will have more light in the core or envelope, respectively. We see in Figure 4 that both core- and envelope-dominated CCGs tend to be at the higher end of the  $R_{\text{eff}}$  values, while core+envelope CCGs tend to be at the lower  $R_{\text{eff}}$  val-

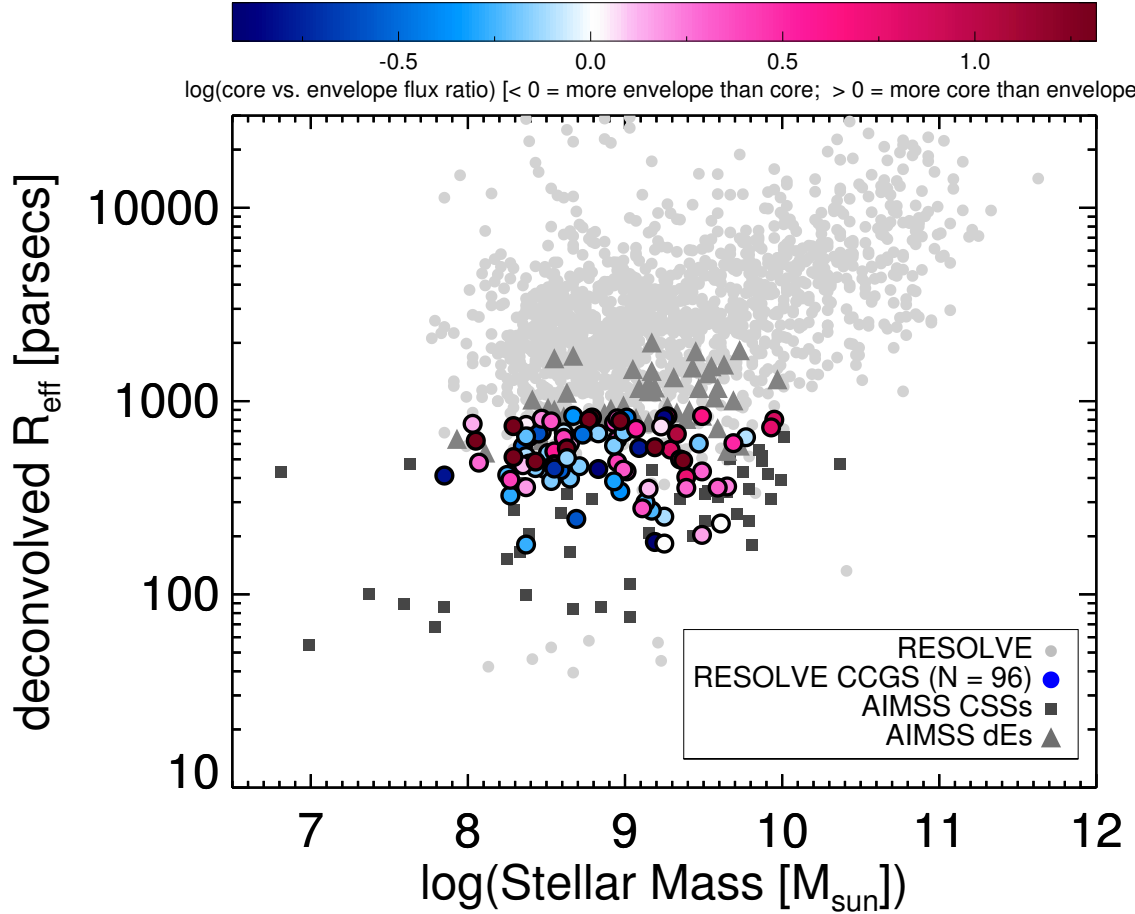


**Figure 4.** The deconvolved  $R_{\text{eff}}$  measurements for the entire RESOLVE sample, along with the CSSs of the AIMSS catalog. In grey are the RESOLVE (non-CCG) galaxies, which are plotted using their one component fit  $R_{\text{eff}}$ . The CCG sample is plotted using the core  $R_{\text{eff}}$  of the two component fits, which is why they may appear separated from the full RESOLVE sample. The colors of the CCGs represent the logarithm of the flux ratio between the core and envelope. Galaxies with  $\log(\text{flux ratio}) \approx 0$  will have both a core and envelope, while galaxies with  $\log(\text{flux ratio}) > 1$  will have more light in the core and  $\log(\text{flux ratio}) < -1$  will have more light in the envelope.

ues. There are also more core-dominated CCGs at the higher  $M_*$  end while envelope-dominated CCGs tend to reside at low  $M_*$ .

#### 4.2. Colors and Star formation rates

We now examine the colors of the CCG sample. The left side of Figure 5 shows the k-corrected and extinction-corrected  $u-r$  colors (as described in § 3.1) of our CCG sample plotted against  $M_*$ , compared to the RESOLVE sample as a whole. An unusual finding is that many CCGs live on the blue sequence, since most CSSs are most often thought of as being “red and dead”. The right side of Figure 5 shows FS-MGR vs.  $M_{\text{bary}}$  for the same objects. As with the colors, we find that many CCGs are forming stars at a rapid rate (FS-MGR  $\sim 1$  means that the galaxy has doubled its mass in the last Gyr), again an unexpected finding which could indicate that some CCGs are still in the process of forming (if dissipatively formed) or relaxing (if tidally-stripped remnants).

#### 4.3. Environments

We next investigate the distribution of CCGs throughout the cosmic web, and find that CCGs span a range of different environments (see Figure 6). There are many CCGs residing

in low mass groups, similar to the M32–Andromeda relationship, which suggests that tidal stripping could have occurred for those CCGs. On the opposite end, we see several CCGs in massive group halos, and these CCGs tend to be either core- or envelope dominated. This hints towards ram pressure stripping being at play in these environments, especially for those CCGs at larger distances from other galaxies. There are also nine CCGs that are  $> 1$  Mpc away from another object in RA-Dec-redshift space, and four of those are core dominated, resembling the isolated cE found by Huxor et al. (2013). These free floating CCGs may be the result of dissipative formation since there is no nearby object to have performed the stripping. Alternatively, they may have been ejected from groups or clusters during the stripping process.

#### 4.4. Kinematics

We lastly investigate the kinematics of the CCG sample using  $\sigma$  values derived from SOAR and Gemini telescope data. Figure 7 plots the Faber-Jackson ( $\sigma$ - $M_*$ ) relation for the eight CCGs with  $\sigma$  measurements along with the other 80+ RESOLVE galaxies with  $\sigma$  measured. Galaxies with  $\sigma$  offset to higher values point to tidal stripping occurring, since they will have less stellar mass than the motions suggest

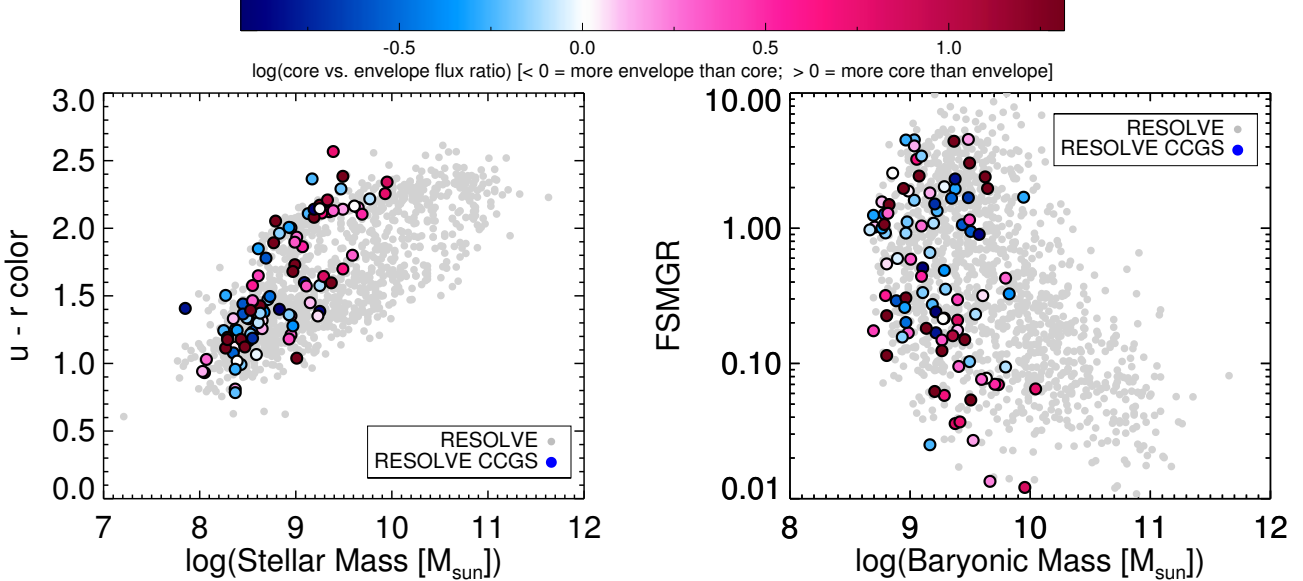


**Figure 5.** (Left.) The  $u-r$  colors against stellar mass of CCGs with the entire RESOLVE sample. (Right.) FSMGR against baryonic mass for both the CCGs and entire RESOLVE sample.

should be there. Conversely, galaxies with  $\sigma$  that lie on the trend may point dissipative formation occurring, since these will have formed similarly to normal elliptical galaxies. Most CCGs seem to be following the dissipative merger track, and in § 5, we examine in depth the formation scenarios for each of these eight CCGs with velocity dispersion measurements.

## 5. CCG FORMATION PROCESSES

We now take an in depth look at the eight CCGs with kinematics, and assign formation scenarios based on their core  $R_{\text{eff}}$  morphology, star formation histories, kinematics, and environments. For this discussion, we classify CCGs using the terms “CSS-like”, “dE-like”, or “crossover”. A CSS-like CCG will have a small core radius and a  $\sigma$  value offset from the main Faber-Jackson relation, as expected for UCDs and cEs that have been tidally stripped. A dE-like CCG will have a large core radius and low  $\sigma$  as is expected for dEs that are dissipatively formed. Crossover CCGs will have small core radius and low  $\sigma$ . Following this logic, we classify M32 as CCS-like since it has  $R_{\text{eff}} \sim 100$  pc and  $\sigma$  offset to higher dispersion. The cE discovered in Huxor et al. (2013) is a crossover, since it has  $R_{\text{eff}} \sim 500$  pc and a  $\sigma$  value falling along the main Faber-Jackson relation.

We have replotted Figures 4, 5, and 6 in Figure 8, this time highlighting the CCGs with velocity dispersions only. An important caveat for the CSSs and dEs in the AIMSS catalog is that the radius measurements are not decomposed into one and two components. To correct for this, we plot in the top left panel of Figure 8 the one component  $R_{\text{eff}}$  instead of the two component core  $R_{\text{eff}}$  so that we may accurately compare the radius measurements of CCGs to those of the AIMSS objects.

### 5.1. dE-like CCGs

We classify rs0345, rs1100, rf0003, and rf0328 as dE-like CCGs, based on their large one-component  $R_{\text{eff}}$  and low  $\sigma$ . The CCGs rs0345 and rs1100 are both envelope-dominated, live firmly on the blue sequence, and are forming

stars quite rapidly with  $\text{FSMGR} > 1$ . The galaxies reside in intermediate-sized groups (halo masses  $\sim 10^{11.7-12.5} M_{\odot}$ ) and are both within  $< 0.15$  Mpc from a companion galaxy. Taken together these data suggest that rs0345 and rs1100 may be an example of a dissipative process actively occurring. Judging from the regular morphologies seen in the images of these CCGs in Figure 9, dissipative formation via merging is unlikely, which leaves ram pressure stripping that is perturbing the gas and fueling star formation as a probable formation scenario given their location in intermediate-sized groups.

CCG rf0003 is core-dominated, lives between the blue and red sequences and has a low  $\text{FSMGR} (\sim 0.10)$ . It resides in a low mass group (halo mass  $\sim 10^{10.9} M_{\odot}$ ) and is  $> 2$  Mpc from another galaxy, which we classify as free floating. Its  $\sigma$  places it firmly along the main Faber-Jackson relation. All together, these clues point to a dissipatively-formed CCG, perhaps through the convergence of cold streams. Residing near the green valley indicate that this formation may have occurred relatively recently.

Lastly, rf0328 is also semi core-dominated and lives intermediate between the blue and red sequences, but has a higher  $\text{FSMGR}$  at  $\sim 0.6$ , indicating considerable star formation taking place in the last Gyr. The galaxy resides in a low mass group and is  $\sim 0.4$  Mpc from a neighbor. Its  $\sigma$  places it among the dissipatively-formed CCGs, perhaps due to ram pressure stripping or even a minor merger. Like rf0003, its color and  $\text{FSMGR}$  may indicate recent formation.

These dE-like CCGs with high  $\text{FSMGR}$  may be related to luminous compact blue dwarfs (LCBDs; Lisker et al. 2013; Crawford et al. 2016) or “green pea” galaxies that were discovered by the Galaxy Zoo project (Cardamone et al. 2009). Green peas have similar sizes and masses as LCBDs but have extreme star formation that cause them to appear green in SDSS  $gri$  image stacks due to huge [OIII] emission lines.

### 5.2. CSS-like CCGs

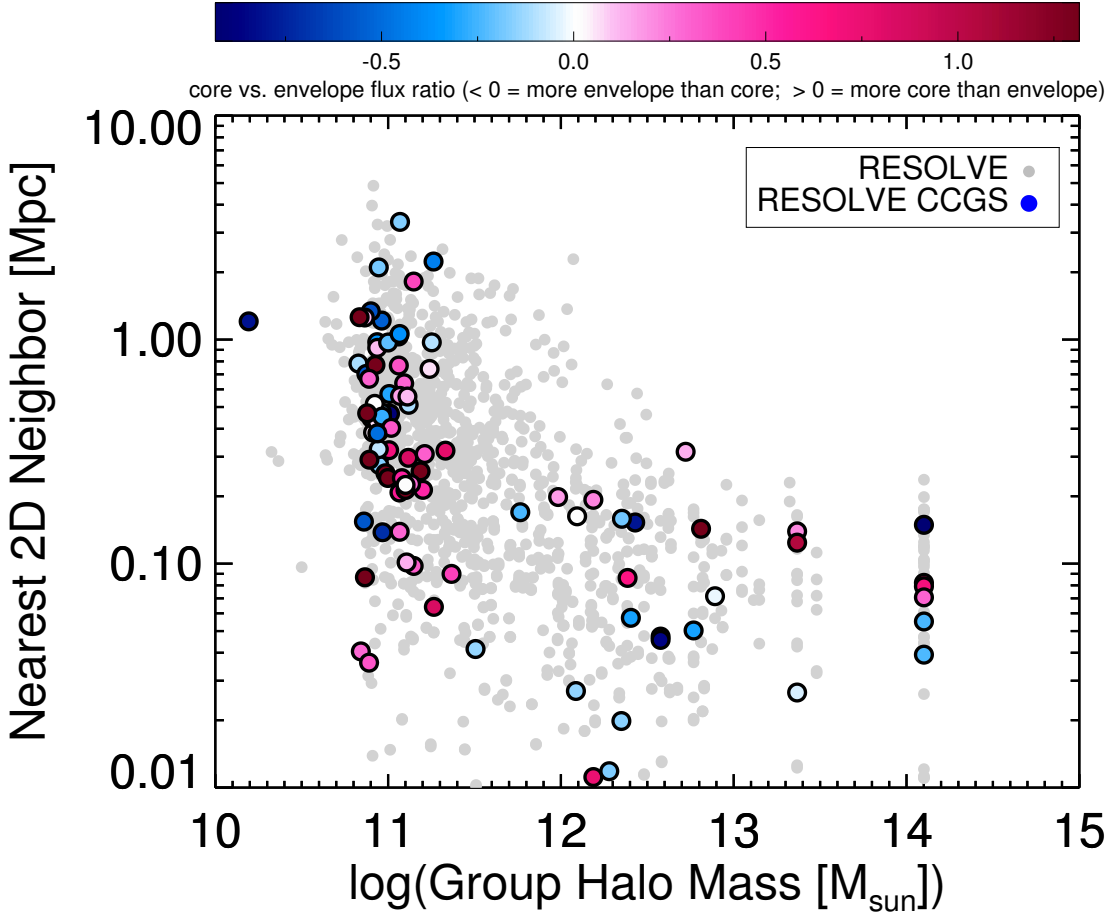


**Figure 6.** Group halo mass vs. the nearest 2D neighbor for the RESOLVE survey and CCG sample. We see that CCGs live in a variety of environments, from extremely isolated (nearest neighbor > 1 Mpc) to massive ( $M_{\text{halo}} \sim 10^{13} M_{\odot}$ ) groups. There is no obvious trend into whether cores+envelopes and cores/envelopes preferentially live in different environments.

We do not find any CSS-like CCGs in our subset of CCGs with kinematic data, however we expect that with additional velocity dispersion data, we will find CCGs following this track in the future.

### 5.3. Crossover CCGs

We classify rs0567, rs1186, rf0078, rf0492 as crossover CCGs, based on their small one component  $R_{\text{eff}}$  measurements ( $\sim 500$ – $700$  pc) and  $\sigma$  values following the dissipative formation track. There are two cEs in AIMSS with extremely small  $R_{\text{eff}}$  and low  $\sigma$  (the dark squares at  $M_{\star} \sim 10^{8.5} M_{\odot}$  and  $\sigma \sim 20 \text{ km s}^{-2}$  in Figure 7), and we classify these as crossovers as well.

The CCGs rs0567, rs1186, and rf0078 are all three mildly core-dominated galaxies. They live on the red sequence and display little star formation ( $\text{FSMGR} > 0.1$ ). CCGs rs1186 and rf0078 both have close neighbors ( $\sim 0.2$  Mpc distance), but rs0567 has a nearest neighbor  $\sim 0.7$  Mpc, which makes it quite similar to the free floating cE discovered by Huxor et al. (2013) (which also has a core-dominated light profile).

CCG rf0492 lies closest to the free floating cE from Huxor et al. (2013) in both Figure 7 and the top left of Figure 9, but they do not share many other similarities. This CCG has a core+envelope profile and lives in an intermediate-sized group

with halo mass  $\sim 10^{12} M_{\odot}$  and neighbor within  $\sim 0.11$  Mpc. It lives on the red sequence and has low FSMGR ( $< 0.1$ ), making it a good candidate of a CCG formed via ram pressure stripping as a dwarf fell into the group halo. The core may have been formed through this process as gas funnels to the center or may have been in place before infalling.

We postulate that CCGs like these may be the low- $z$  analogues to the “red/blue nugget” galaxies that are common at high-redshift with  $R_{\text{eff}} < 1$  kpc. Dekel & Burkert (2013) propose that at high redshifts, blue nuggets form when gaseous disks contract during dissipative processes and then later quench to become red nuggets that are so common in the early universe.

## 6. CONCLUSIONS

In this paper we have examined the morphologies, colors, FSMGR, environments, and kinematics of the 96 compact core galaxies (CCGs) in the RESOLVE survey. We have selected CCGs to have a seeing-deconvolved, core-only  $R_{\text{eff}} < 800$  pc, based on the sizes of the compact and dwarf ellipticals in the AIMSS catalog. We quantified the morphology of CCGs by performing two component (core and envelope) Sérsic fits with GALFIT and taking the logarithm of the ratio of the fluxes of the core and the envelope. CCGs with more light in the envelope have  $\log(\text{flux ratio}) < 0$  and are called

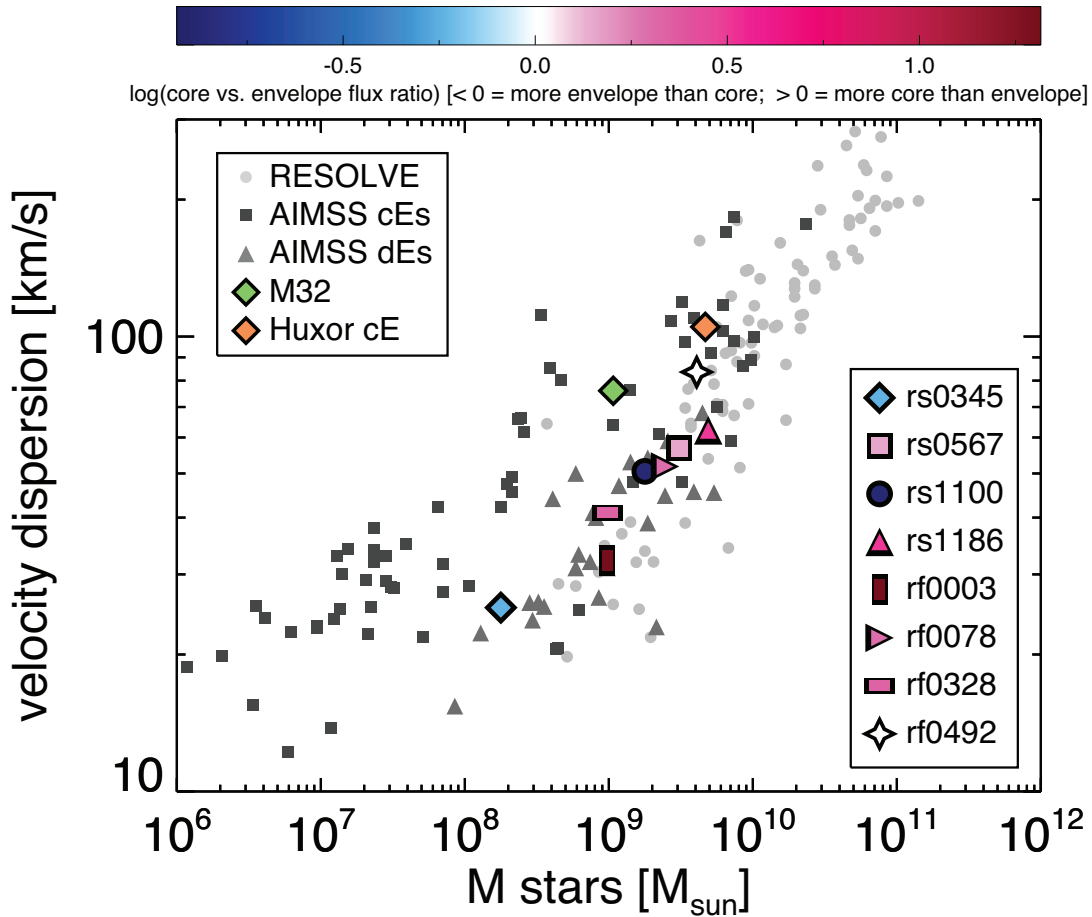


**Figure 7.** The Faber-Jackson relation (stellar mass vs. velocity dispersion) for the RESOLVE sample, CCGs, and the cEs and dEs of the AIMSS catalog. We look for CCGs offset to higher  $\sigma$  for its stellar mass, which may indicate tidal stripping as a possible formation scenario. The green point is M32, the prototypical cE, that is believed to be tidally stripped (Faber 1973). In orange is the free floating cE discovered in Huxor et al. (2013) that is thought to be dissipatively formed.

“envelope-dominated” CCGs. CCGs with more light in the core have  $\log(\text{flux ratio}) > 0$  and are called “core-dominated” CCGs. CCGs with  $\log(\text{flux ratio}) \sim 0$  have both a bright core plus an extended envelope and are called “core+envelope” CCGs. Our main results can be summarized as follows:

1. [Figure 4](#) shows that both core- and envelope-dominated CCGs tend to be at the higher end of the  $R_{\text{eff}}$  values, while core+envelope CCGs tend to be the lower  $R_{\text{eff}}$  values. There also are more core-dominated CCGs at the higher  $M_*$  end while envelope-dominated CCGs tend to reside at low  $M_*$ .
2. We find that many CCGs live on the blue sequence and are forming stars at a rapid rate (see [Figure 5](#)), which could indicate that some CCGs are still in the process of forming (if dissipatively formed) or relaxing (if a tidally-stripped remnant).
3. We find that CCGs span a range of different environments (see [Figure 6](#)). Many CCGs live in low mass groups, similar to the M32–Andromeda relationship, perhaps hinting at tidal stripping formation scenarios. Others live in massive group halos where tidal or ram pressure stripping may occur. There are also many CCGs that are  $> 1$  Mpc away from another object in RA–Dec–redshift space, resembling the free floating cEs found by [Huxor et al. \(2013\)](#) and [Paudel et al. \(2014\)](#), which may point to dissipative formation scenarios or tidally stripped CCGs that have been ejected.
4. Using velocity dispersions ( $\sigma$ ) derived from the SOAR and Gemini telescopes, we classify the eight CCGs with  $\sigma$  measurements as “CCS-like”, “dE-like”, or “crossover”, based on their position in the Faber–Jackson ( $\sigma$ - $M_*$ ) relation ([Figure 7](#)) and one-component radius measurements (the top left panel of [Figure 8](#)). We find four CCGs that are dE-like and four that are crossovers.

Future work will include the following:

1. *Redefine CCG sample using  $\chi^2$  analysis.* As mentioned in § 2.3.2, we want to redefine the CCG sample using the  $\chi^2$  and number of degrees of freedom (NoDF) output by GALFIT for each fit. This will entail using the  $\chi^2$  and NoDF to decide whether the one or two component fits are best for all RESOLVE galaxies. Those best fit with one component would then be selected as a CCG if its one component  $R_{\text{eff}}$  is less than 800 pc, while those best fit with two components would be selected as a CCG if its core  $R_{\text{eff}}$  is less than 800 pc. This method replace the arbitrary cutoff for CCG candidates at  $R_{\text{eff}} < 1$  kpc, which should let us include more CCGs that have large diffuse envelopes and small cores that may be getting left out of our sample now.
2. *Investigate gas content.* The amount of neutral hydrogen gas CCGs have may give us insight into their evolution over time. For example, a CCG in a galaxy cluster with little HI gas may point towards ram pressure stripping being important. Combined with CCG colors and FSGMR, gas content may be an important diagnostic in determining the evolution of a CCG.

3. *Investigate metallicities.* [Janz et al. \(2015\)](#) have shown that tidally-stripped CSSs are systematically offset to higher metal abundances. With the SOAR and Gemini spectroscopy currently in hand, we will be able to test this hypothesis for the CCG sample and use this method as another way to discern formation scenarios.

*Acknowledgments.* This work has been supported by funding from NSF grants AST-0955368 and OCI-1156614 and NASA grant HST-AR-12147.01-A. This work is based on data obtained as part of the UKIRT Infrared Deep Sky Survey. This work is based on observations obtained at the Gemini Observatory under program numbers GS-2013B-Q52, GS-2014B-Q-13, GS-2014B-Q-51, and GS-2015B-C-1, which is operated by the Association of Universities for Research in Astronomy, Inc., under a cooperative agreement with the NSF on behalf of the Gemini partnership: the National Science Foundation (United States), the National Research Council (Canada), CONICYT (Chile), Ministerio de Ciencia, Tecnología e Innovación Productiva (Argentina), and Ministério da Ciência, Tecnologia e Inovação (Brazil).

## REFERENCES

- Aihara, H., Allende Prieto, C., An, D., et al. 2011, The Astrophysical Journal Supplement Series, 193, 29
- Bekki, K., Couch, W. J., & Drinkwater, M. J. 2001, The Astrophysical Journal, 552, L105
- Bekki, K., & Freeman, K. C. 2003, Monthly Notices of the Royal Astronomical Society, 346, L11
- Bender, R., Burstein, D., & Faber, S. M. 1992, The Astrophysical Journal, 399, 462
- Berlind, A. A., Frieman, J., Weinberg, D. H., et al. 2006, The Astrophysical Journal Supplement Series, 167, 1
- Bertin, E., & Arnouts, S. 1996, Astronomy and Astrophysics Supplement Series, 117, 393
- Binggeli, B., & Cameron, L. M. 1991, Astronomy and Astrophysics (ISSN 0004-6361), 252, 27
- Binggeli, B., Sandage, A., & Tarenghi, M. 1984, The Astronomical Journal, 89, 64
- Blanton, M. R., & Berlind, A. A. 2007, The Astrophysical Journal, 664, 791
- Blanton, M. R., Kazin, E., Muna, D., Weaver, B. A., & Price-Whelan, A. 2011, The Astronomical Journal, 142, 31
- Cappellari, M., & Emsellem, E. 2004, Publications of the Astronomical Society of the Pacific, 116, 138
- Cardamone, C., Schawinski, K., Sarzi, M., et al. 2009, Monthly Notices of the Royal Astronomical Society, 399, 1191
- Chilingarian, I., Cayatte, V., Revaz, Y., et al. 2009, Science (New York, N.Y.), 326, 1379
- Chilingarian, I., & Zolotukhin, I. 2015, Science (New York, N.Y.), 348, 418
- Chilingarian, I. V., & Bergond, G. 2010, Monthly Notices of the Royal Astronomical Society: Letters, 405, L11
- Chilingarian, I. V., Sil’chenko, O. K., Afanasiev, V. L., & Prugniel, P. 2007, Astronomy Letters, 33, 292
- Choi, P. I., Guhathakurta, P., & Johnston, K. V. 2002, The Astronomical Journal, 124, 310
- Clemens, J. C., Crain, J. A., & Anderson, R. 2004, in Ground-based Instrumentation for Astronomy. Edited by Alan F. M. Moorwood and Iye Masanori. Proceedings of the SPIE, ed. A. F. M. Moorwood & M. Iye, Vol. 5492, 331–340
- Colless, M., Dalton, G., Maddox, S., et al. 2001, Monthly Notices of the Royal Astronomical Society, 328, 1039
- Crawford, S. M., Wirth, G. D., Bershadsky, M. A., & Randriamampandry, S. M. 2016, The Astrophysical Journal, 817, 87
- Crnojević, D., Ferguson, A. M. N., Irwin, M. J., et al. 2014, Monthly Notices of the Royal Astronomical Society, 445, 3862
- Dekel, A., & Burkert, A. 2013, Monthly Notices of the Royal Astronomical Society, 438, 1870
- Drinkwater, M. J., Jones, J. B., Gregg, M. D., & Phillipps, S. 2000, Publications of the Astronomical Society of Australia, 17, 227
- Driver, S. P., Hill, D. T., Kelvin, L. S., et al. 2011, Monthly Notices of the Royal Astronomical Society, 413, 971
- Eckert, K. D., Kannappan, S. J., Stark, D. V., et al. 2016, eprint arXiv:1604.03957
- . 2015, The Astrophysical Journal, 810, 166
- Evstigneeva, E. A., Drinkwater, M. J., Jurek, R., et al. 2007, Monthly Notices of the Royal Astronomical Society, 378, 1036

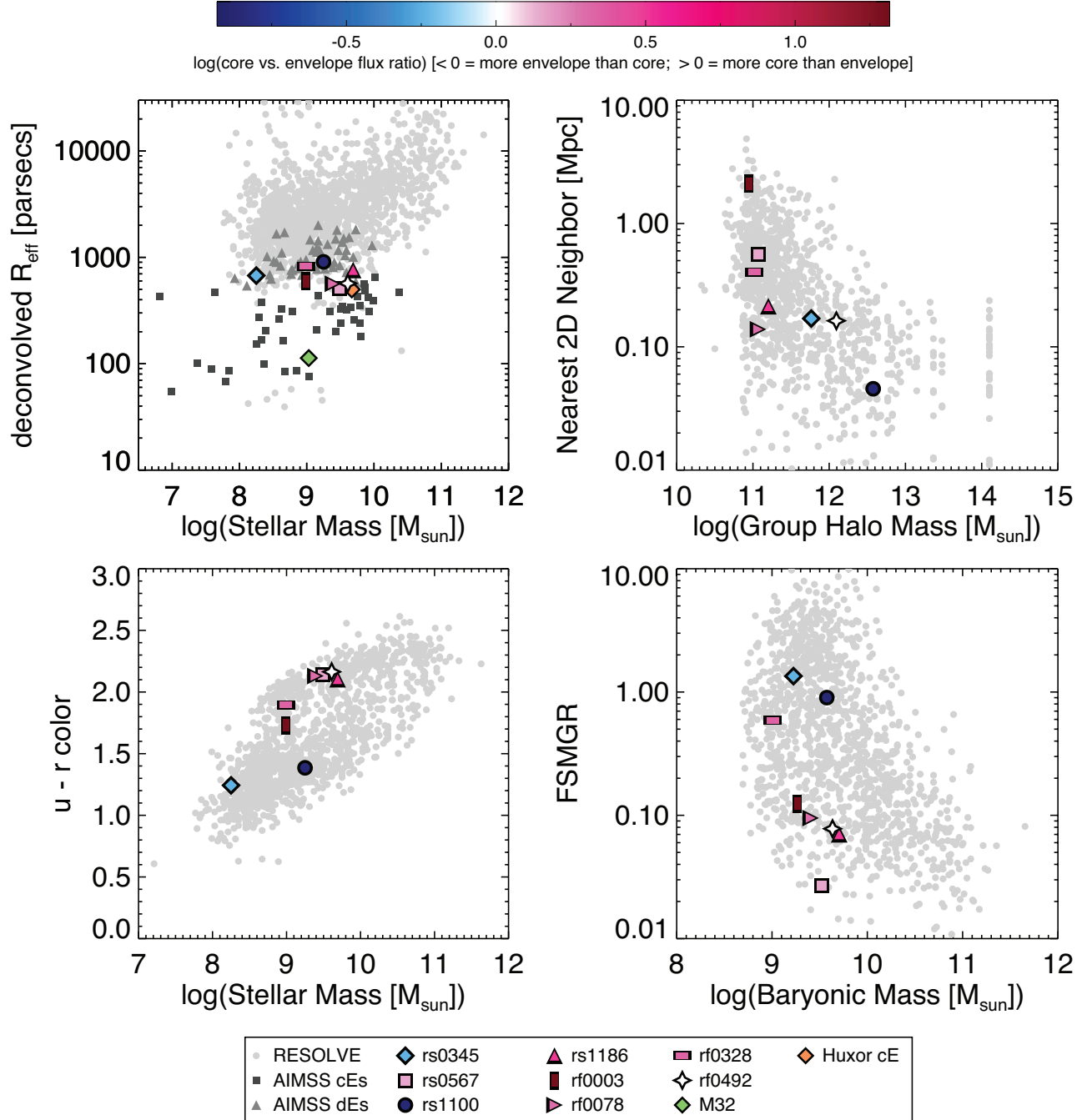


**Figure 8.** (Top left.) single-component deconvolved  $R_{\text{eff}}$  vs. stellar mass, (Top right.) the nearest two-dimensional neighbor vs. group halo mass, (Bottom left.)  $u - r$  color vs. stellar mass, and (Bottom right.) FSMGR vs. baryonic mass for all galaxies in RESOLVE, the cEs and dEs of AIMSS, and the eight CCGs that have velocity dispersion information. We emphasize that the  $R_{\text{eff}}$  values plotted in the top left panel are not the two-component core  $R_{\text{eff}}$  values as in Figure 4 in order to compare our radius measurements with the CSSs of AIMSS that have not been decomposed.

- Faber, S. M. 1973, *The Astrophysical Journal*, 179, 423
- Faber, S. M., & Jackson, R. E. 1976, *The Astrophysical Journal*, 204, 668
- Falco, E., Kurtz, M., Geller, M., et al. 1999, *Publications of the Astronomical Society of the Pacific*, 111, 438
- Ferrarese, L., Côté, P., Dalla Bontà, E., et al. 2006, *The Astrophysical Journal*, 644, L21
- Forbes, D. A., Norris, M. A., Strader, J., et al. 2014, *Monthly Notices of the Royal Astronomical Society*, 444, 2993
- Graham, A. W. 2002, *The Astrophysical Journal*, 568, L13
- Grant, N. I., Kuipers, J. A., & Phillipps, S. 2005, *Monthly Notices of the Royal Astronomical Society*, 363, 1019
- Greisen, E. W., & Calabretta, M. R. 2002, *Astronomy and Astrophysics*, 395, 1061
- Guzmán, R., Koo, D. C., Faber, S. M., et al. 1996, *The Astrophysical Journal*, 460, doi:10.1086/309966
- Hau, G. K. T., Spitler, L. R., Forbes, D. A., et al. 2009, *Monthly Notices of the Royal Astronomical Society: Letters*, 394, L97
- Haynes, M. P., Giovanelli, R., Martin, A. M., et al. 2011, *The Astronomical Journal*, 142, 170
- Hilker, M., Infante, L., Vieira, G., Kissler-Patig, M., & Richtler, T. 1999, *Astronomy and Astrophysics Supplement Series*, 134, 75
- Huxor, A. P., Phillipps, S., & Price, J. 2013, *Monthly Notices of the Royal Astronomical Society*, 430, 1956
- Huxor, A. P., Phillipps, S., Price, J., & Harniman, R. 2011, *Monthly Notices of the Royal Astronomical Society*, 414, 3557
- Janz, J., Norris, M. A., Forbes, D. A., et al. 2015, *Monthly Notices of the Royal Astronomical Society*, 456, 617
- Jennings, Z. G., Romanowsky, A. J., Brodie, J. P., et al. 2015, *The Astrophysical Journal*, 812, L10
- Jones, D. H., Read, M. A., Saunders, W., et al. 2009, *Monthly Notices of the Royal Astronomical Society*, 399, 683
- Jones, J. B., Drinkwater, M. J., Jurek, R., et al. 2006, *The Astronomical Journal*, 131, 312
- Kannappan, S. J., Wei, L. H., Minchin, R., & Momjian, E. 2008, in *AIP Conference Proceedings*, Vol. 1035 (AIP), 163–168
- Kannappan, S. J., Stark, D. V., Eckert, K. D., et al. 2013, *The Astrophysical Journal*, 777, 42
- Koo, D. C., Bershady, M. A., Wirth, G. D., Stanford, S. A., & Majewski, S. R. 1994, *The Astrophysical Journal*, 427, L9
- Kormendy, J., & Bender, R. 2012, *The Astrophysical Journal Supplement Series*, 198, 2
- Kormendy, J., Fisher, D. B., Cornell, M. E., & Bender, R. 2009, *The Astrophysical Journal Supplement Series*, 182, 216
- Kormendy, J., Bender, R., Magorrian, J., et al. 1997, *The Astrophysical Journal*, 482, L139
- Lawrence, A., Warren, S. J., Almaini, O., et al. 2007, *Monthly Notices of the Royal Astronomical Society*, 379, 1599
- Lisker, T., Weinmann, S. M., Janz, J., & Meyer, H. T. 2013, *Monthly Notices of the Royal Astronomical Society*, 432, 1162
- Liu, C., Peng, E. W., Côté, P., et al. 2015, *The Astrophysical Journal*, 812, 34
- Madrid, J. P., Graham, A. W., Harris, W. E., et al. 2010, *The Astrophysical Journal*, 722, 1707
- Maraston, C., Bastian, N., Saglia, R. P., et al. 2004, *Astronomy and Astrophysics*, 416, 467
- Maraston, C., & Strömbäck, G. 2011, *Monthly Notices of the Royal Astronomical Society*, 418, 2785
- Mastropietro, C., Moore, B., Mayer, L., et al. 2005, *Monthly Notices of the Royal Astronomical Society*, 364, 607
- Mieske, S., Hilker, M., & Infante, L. 2002, *Astronomy and Astrophysics*, 383, 823
- Mieske, S., Hilker, M., Misgeld, I., et al. 2009, *Astronomy and Astrophysics*, 498, 705
- Misgeld, I., Mieske, S., & Hilker, M. 2008, *Astronomy and Astrophysics*, 486, 697
- Morrissey, P., Conrow, T., Barlow, T. A., et al. 2007, *The Astrophysical Journal Supplement Series*, 173, 682
- Norris, M. A., & Kannappan, S. J. 2011, *Monthly Notices of the Royal Astronomical Society*, 414, 739
- Norris, M. A., Kannappan, S. J., Forbes, D. A., et al. 2014, *Monthly Notices of the Royal Astronomical Society*, 443, 1151
- Oser, L., Ostriker, J. P., Naab, T., Johansson, P. H., & Burkert, A. 2010, *The Astrophysical Journal*, 725, 2312
- Paturel, G., Petit, C., Prugniel, P., et al. 2003, *Astronomy and Astrophysics*, 412, 45
- Paudel, S., Lisker, T., Hansson, K. S. A., & Huxor, A. P. 2014, *Monthly Notices of the Royal Astronomical Society*, 443, 446
- Peng, C. Y., Ho, L. C., Impey, C. D., & Rix, H.-W. 2002, *The Astronomical Journal*, 124, 266
- Penny, S. J., Forbes, D. A., Pimbblet, K. A., & Floyd, D. J. E. 2014, *Monthly Notices of the Royal Astronomical Society*, 443, 3381
- Pfeffer, J., & Baumgardt, H. 2013, *Monthly Notices of the Royal Astronomical Society*, 433, 1997
- Phillipps, S., Drinkwater, M. J., Gregg, M. D., & Jones, J. B. 2001, *The Astrophysical Journal*, 560, 201
- Price, J., Phillipps, S., Huxor, A., et al. 2009, *Monthly Notices of the Royal Astronomical Society*, 397, 1816
- Sandage, A., Binggeli, B., & Tammann, G. A. 1985, *The Astronomical Journal*, 90, 1759
- Sandoval, M. A., Vo, R. P., Romanowsky, A. J., et al. 2015, *The Astrophysical Journal*, 808, L32
- Sérsic, J. L. 1963, *Boletin de la Asociacion Argentina de Astronomia La Plata Argentina*, 6, 41
- . 1968, *Cordoba, Argentina: Observatorio Astronomico*, 1968
- Seth, A. C., van den Bosch, R., Mieske, S., et al. 2014, *Nature*, 513, 398
- Skrutskie, M. F., Cutri, R. M., Stiening, R., et al. 2006, *The Astronomical Journal*, 131, 1163
- Smith Castelli, A. V., Cellone, S. A., Faifer, F. R., et al. 2012, *Monthly Notices of the Royal Astronomical Society*, 419, 2472
- Smith Castelli, A. V., Faifer, F. R., Richtler, T., & Bassino, L. P. 2008, *Monthly Notices of the Royal Astronomical Society*, 391, 685
- van Dokkum, P. G. 2001, *Publications of the Astronomical Society of the Pacific*, 113, 1420
- Wirth, A., & Gallagher, J. S., I. 1984, *The Astrophysical Journal*, 282, 85
- York, D. G., Adelman, J., Anderson, Jr., J. E., et al. 2000, *The Astronomical Journal*, 120, 1579
- Zhang, H.-X., Peng, E. W., Côté, P., et al. 2015, *The Astrophysical Journal*, 802, 30

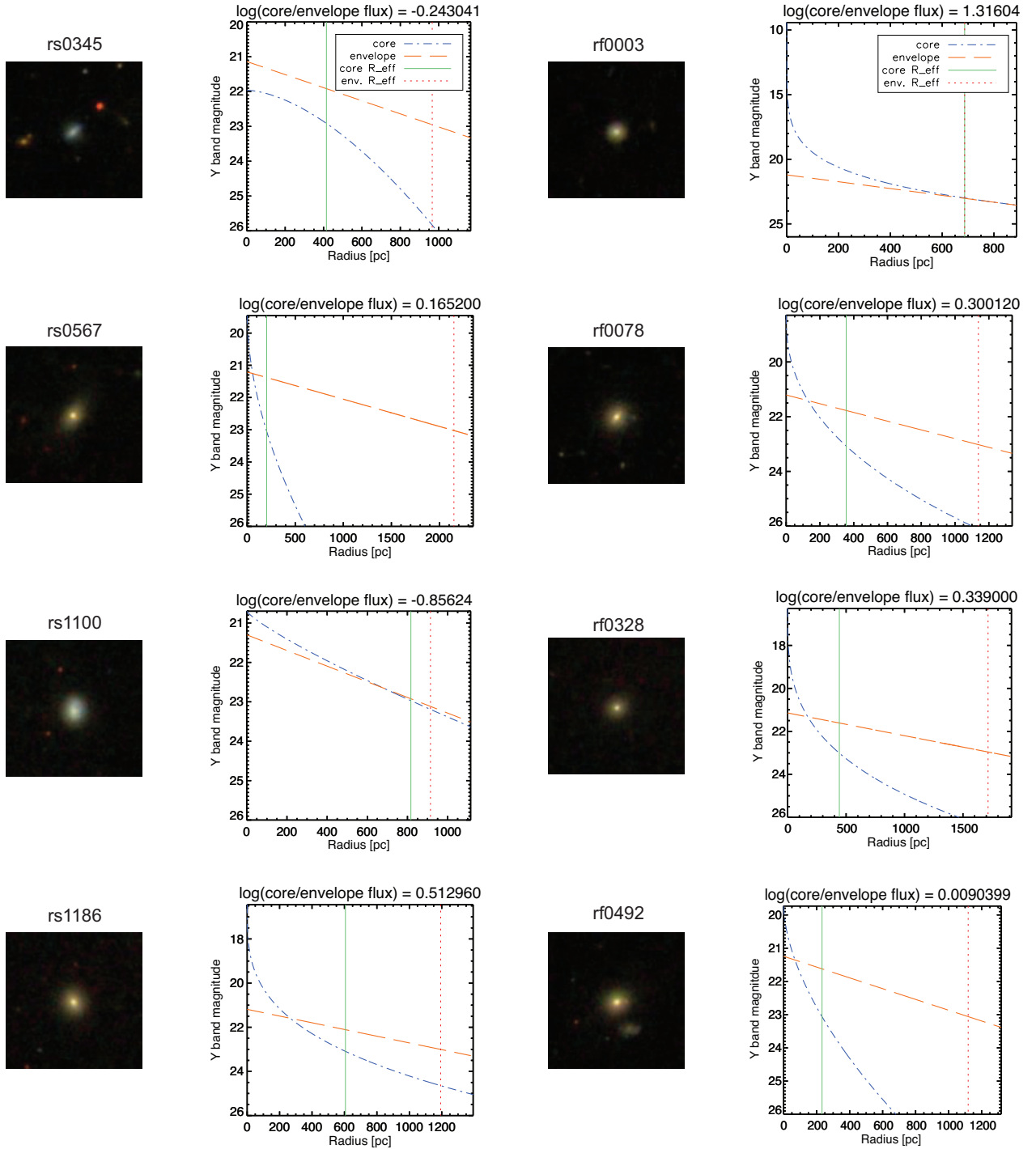


**Figure 9.** The light profiles for the eight CCGs with velocity dispersion measurements. The *rgb* images are from the SDSS-DR8 image list tool. Above each plot is the value of the logarithm of the ratio of the core and envelope fluxes, which are given via the symbol colors in Figure 7 and Figure 8. We also note that rf0003 is one of the six cases where GALFIT finds identical  $R_{\text{eff}}$  values for both the first and second Sérsic components, and have hence set  $\log(\text{flux ratio}) = \text{maximum}$  of all flux ratios (+1.31).

# Appendix: Gemini-South IFU Data Reduction User Manual

Elaine M. Snyder  
Dept. of Physics & Astronomy  
University of North Carolina at Chapel Hill  
`emsnyder@live.unc.edu`

February 22, 2016

# Contents

<b>1</b>	<b>Introduction</b>	<b>3</b>
1.1	What is an IFU and why would we want to use one? . . . . .	3
1.2	Observing setups . . . . .	3
1.3	Observing patterns . . . . .	4
1.4	Files you'll need for reduction . . . . .	5
1.5	How the data is stored . . . . .	5
1.5.1	The raw fits files . . . . .	5
1.5.2	What is an MDF? . . . . .	5
<b>2</b>	<b>Setting Up Your Workspace</b>	<b>9</b>
<b>3</b>	<b>Data Reduction Guide</b>	<b>11</b>
3.1	How to Use This Guide . . . . .	11
3.2	Entering and Exiting the Pipeline . . . . .	11
3.3	Organizing and Identifying Your Data . . . . .	11
3.4	Bias + Overscan Subtraction and Trimming of the Flats and Fiber Identification . . . . .	12
3.5	Overscan Subtraction and Trimming of the Arcs . . . . .	14
3.6	Bias + Overscan Subtraction and Trimming of Science Data . . . . .	14
3.7	Identification and Removal of Bad Pixels from the Science, Flats, and Arcs . . . . .	15
3.8	Extraction of the Arcs . . . . .	16
3.9	Creation of the Wavelength Solution . . . . .	17
3.10	Application of the Calibration to the Arcs . . . . .	18
3.11	Quantum Efficiency Correction of the Flats . . . . .	19
3.12	Re-extraction of the Flats . . . . .	19
3.13	Creation of the Response Functions . . . . .	19
3.14	Quantum Efficiency Correction of the Arcs . . . . .	19
3.15	Flat Fielding and Extraction of the Arcs . . . . .	20
3.16	Re-creation of the Wavelength Solution for the QE-Corrected & Flat Fielded Arcs . . . . .	20
3.17	Application of the Calibration to the QE-corrected & Flat Fielded Arcs . . . . .	20
3.18	Cosmic Ray Rejection in the Science Data . . . . .	20
3.19	QE Correction of Science . . . . .	20
3.20	Flat Fielding and Extraction of Science . . . . .	20
3.21	Wavelength Calibration of Science . . . . .	20
3.22	Sky Subtraction of Science . . . . .	21
3.23	Flux Calibration of Science . . . . .	21
3.24	Data Cube Creation . . . . .	21
3.25	Creation of a WCS Solution . . . . .	22
3.26	Summation of the Data Cubes . . . . .	22

<b>4 Other Things You'll Want to Know</b>	<b>24</b>
4.1 Creating the Bias Frame . . . . .	24
4.2 Reducing the Twilight and Standard Star Data . . . . .	24
4.3 When Things Go Wrong... . . . . .	26
4.3.1 A Bad Fiber Identification . . . . .	26
4.3.2 A Bad Wavelength Solution . . . . .	27
4.3.3 Correcting the 2014B Data with Bad Amplifier Effects . . . . .	27

## List of Figures

1.1 IFU Fibers and Data Format . . . . .	7
1.2 Example of DS9 cube diaglog box . . . . .	8
1.3 Example of DS9 cube diaglog box . . . . .	8
3.1 Overscan Subtraction Example . . . . .	12
3.2 Examples of the Fiber ID Step . . . . .	14
3.3 Example Image of a Bad Fiber . . . . .	15
3.4 Cosmic Rays vs. Bad Pixels . . . . .	16
3.5 Example of the wavelength solution . . . . .	17
3.6 Example of the residuals of the wavelength fit . . . . .	18
3.7 Before and After Wavelength Calibration . . . . .	19
3.8 Examples of Sky Spectra in the Blue and Red Setups . . . . .	21
3.9 Data Cube Summation Examples . . . . .	23
4.1 Example bias frame . . . . .	25
4.2 Example of the IFU fibers incorrectly identified . . . . .	26
4.3 Example of A Bad Wavelength Transformation . . . . .	28
4.4 Example of the Bad Amplifier Issues in 2014B . . . . .	29
4.5 Another Example of the Bad Amplifier Issues in 2014B . . . . .	30
4.6 The Flat that Corrects the Bad Amplifier Issues . . . . .	31

## List of Tables

1.1 RESOLVE's Observation Setups . . . . .	4
1.2 Order of Observations . . . . .	5

## Chapter 1

### Introduction

Greetings, Gemini Multi-Object Spectrograph (GMOS) integral field unit (IFU) data reduction pipeline user! Before beginning your data reduction journey, it will be important to understand the structure of an IFU and the way the Gemini IFU data is stored in the fits files you'll be reducing. If you are familiar with this already, feel free to skip ahead. Most of this information can be found online on <https://www.gemini.edu>, but I've compiled it all here for easy reference and so that I may reference it in the context of the RESOLVE<sup>1</sup> survey's instrument setups.

#### 1.1 What is an IFU and why would we want to use one?

The basic idea of any spectrograph is that incoming light from an object goes through a slit, is dispersed by a grating/prism/grism, and then focused onto the CCD detector to create an image of the spectrum. Most of the time the slit is long and narrow ( $\sim 0.5\text{--}2''$  typically), and most astronomers would align it along a galaxy's major axis. This image will thus have spectral information in the x direction and spatial information in the y direction. The GMOS IFU is different in that instead of having one slit aligned along a galaxy's major axis, you will have multiple fibers that cover the entire galaxy. These fibers act as "mini slits", and each one will be dispersed and refocused onto the detector. This means you receive spectral information from all parts of the galaxy, not just where a single slit falls, and therefore are getting x, y, and wavelength at once. Thus, the main benefit of using an IFU is that it enables the 3D spatial analysis of the kinematics, metallicities, or whatever else you may want to derive from your spectra.

In the case of the GMOS IFU setups for RESOLVE observations, you will have either 750 or 1500 hexagonal fibers (depending on which setup was used) that cover an on-sky area of  $5'' \times 3.5''$  or  $7'' \times 5''$ . The top-right portion of [Figure 1.1](#) gives an example of the positions of the fibers over a galaxy. As the top left portion of [Figure 1.1](#) shows, the GMOS IFU is designed in such a way that not all of the fibers are centered on the object – either 250 or 500 of the fibers are positioned on a region of sky away from the target (but not too far away). This lets us observe separate spectra of the scattered light from our atmosphere, which can later be subtracted from the science spectra during data reduction. This "sky level" can be affected by moon illumination, clouds, etc. so it is important to be able to subtract any extra light there may be. Note that sometimes in online documents, the fibers may be called "spaxels", which is short for "spectral pixels" – don't be confused by this hip IFU lingo.

#### 1.2 Observing setups

As alluded to before, there are two main setups for RESOLVE's IFU observations. Similarly to our SOAR observations, there is a blue setup for absorption line galaxies and red setup for emission line galaxies. [Table 1.1](#) highlights the main differences between the two setups. To determine which setup is best for which galaxy, we ideally like to use the SOAR broad spectrum as a guide. Seeing strong emission in the broad spectrum will point to the emission line setup on Gemini being best, while no emission will point to the absorption line setup being preferred. However, since there is not always a

---

<sup>1</sup><http://www.resolve.astro.unc.edu>

quantity	blue setup	red setup
wavelength range used for central wavelengths	4200 – 5600 Å	5500 – 6900 Å
features of interest	absorption line galaxies 4850, 4900 Å	emission line galaxies 6300, 6400 Å
grating	H $\beta$ , Mg $b$ , Fe5270, Fe5335	H $\alpha$ , [NII], NaD
filter	B1200	B600
slits	none (open)	r-G0326
field of view	1 slit 3.5" × 5"	2 slits 5" × 7"

Table 1.1: Comparison of RESOLVE’s red and blue observation setups for the Gemini-South IFU.

SOAR (or even an SDSS) spectrum available, we often rely on photometric colors as an indicator of whether emission or absorption is more likely.

Using the GMOS IFU is ideal for RESOLVE’s purposes for two different reasons. In the red setup, our goal is to obtain velocity fields for RESOLVE’s smallest emission line galaxies. Thus, the spatial information we receive from the IFU spectra is ideal for this purpose. On the other hand, for the blue setup, our goal is to derive velocity dispersions. The small, absorption line galaxies we target with the IFU in the blue setup are often quite faint, so instead of focusing on the spatial information the IFU gives, we sum all the spaxels out to the effective radius of the galaxy, thereby summing the light enough to derive accurate dispersion measurements.

We estimate exposure times for both setups using the online Integration Time Calculators<sup>2</sup> (ITC) supplied by Gemini. We use an elliptical galaxy SED template for time estimates in the blue setup and adjust our exposure time calculations so that we may achieve a signal-to-noise ratio of 25 per Å when we bin all the fibers out to the effective radius of the galaxy. We use a model H $\alpha$  line with estimates of the line flux and continuum flux density for time estimates in the red setup, and adjust our exposure times to achieve a centroiding accuracy of  $\sim 5.3 \text{ km s}^{-1}$ . For both setups, we bin our spectra by 2 in the spectral direction to increase the signal-to-noise as well.

We also use the ITC to select central wavelength positions that ensure our features of interest do not fall in a chip gap (see bottom of Figure 1.1). We choose two different central wavelengths so that we can fill in the chip gaps as well when we sum the individual exposures – this is sometimes referred to as “spectral dithering”. The central wavelength positions selected for our setups are listed in Table 1.1.

### 1.3 Observing patterns

In 2-slit (aka red setup) mode, we oftentimes will tile the IFU field of view in order to cover the entire extent of the galaxy. The 5" × 7" field of view can either be tiled to 10" × 7" for larger, rounder galaxies or to 5" × 14" for longer, skinnier galaxies. This doesn’t make a large difference to the reduction routine, but there will be more science frames to reduce and more data cubes to stack at the end.

The basic observation sequence is different for each mode. See Table 1.2 for the basic order of the observations. Both will start with acquisition images to ensure the IFU field of view is centered on the galaxy. Then flats, arcs, and science frames are taken in each wavelength dither (denoted as  $\lambda_{cen}$  in Table 1.2). For example, a flat, arc, science, and arc frame will be taken at one central wavelength, and then an arc, science, arc, flat frame will be taken at the other central wavelength. For the reduction, we will want to flat field and wavelength transform the science images using the arcs and flats taken in the same dither. Once the data cubes are made, we can then sum the data cubes, both spatially and spectrally.

<sup>2</sup><http://www.gemini.edu/node/10479>

$\lambda_{cen}$	blue setup	time	red setup	$\lambda_{cen}$
—	acquisition images		acquisition images	—
4850 Å	galaxy flat arc		flat arc galaxy	6300 Å
4900 Å	arc flat galaxy		galaxy arc flat	6400 Å
←				

Table 1.2: Comparisons of the order in which the data for each galaxy is observed in each setup.

## 1.4 Files you'll need for reduction

The fits files you'll want for your data reduction can all be found online in the Gemini Science Archive (<http://archive.gemini.edu>). You will have to create an account with your unique observing program ID and program key (usually sent in an email for each new semester). RESOLVE's IDs are GS-2013B-Q-51 for the fall 2013 semester, GS-2014B-Q-13 and GS-2014B-Q-52 for the fall 2014 semester, and GS-2015B-C-1 (and carry-over GS-2014B-Q-13 band 1 time) for the fall 2015 semester (email Elaine or Sheila<sup>3</sup>, if you need the program keys for any of these programs). Once your account is created, you can look at each observing program and download the data you want.

As alluded to in § 1.3, you'll have flats, arcs, and science data for each galaxy in each wavelength dither. Normally, there are 2 flats, 2 or 4 arcs, and 2 or 4 science frames, depending on the estimated exposure times and/or the spatial offsets needed.

We'll next want a bias image in order to perform the bias subtraction. The process for making the bias frame is explained in § 4.1.

We also obtain a suite of baseline standards each semester – one standard for both the red and blue setups that will be used for each galaxy observation taken that semester. This includes a science observation of a standard star along with flats, arcs, and twilight flats in both wavelength dithers. We use the twilight flats to create response functions for each fiber in the IFU, and use the standard star science observations to correctly flux calibrate our galaxy data. See § 4.2 for how to create the response function and flux calibration files.

## 1.5 How the data is stored

### 1.5.1 The raw fits files

Simply opening one of the S....fits files with DS9 will yield a strange result. You'll see a very long and skinny image appear. What you are actually seeing is 1/12th of the full image. This is because there are 3 CCDs and each one has 4 individual amplifiers that are read out into different extensions in your fits file. To see all the extensions, type `ds9 -mecube S....fits`, which will open a cube dialog box that lets you scroll through each extension in the file. See Figure 1.2 and Figure 1.3 as an example of what you'll see when you open a raw image. A part of the data reduction is to mosaic all of these extensions onto one single large image.

### 1.5.2 What is an MDF?

The mask definition file (MDF) stores information about the IFU and is “attached” to the raw images as one of the first steps in the data reduction process. The actual file is in binary fits format and comes with the Gemini IRAF package. The files are called either “gsifu\_slitr\_mdf.fits” or “gsifu\_slits\_mdf.fits” for the 1- and 2-slit data, respectively, and can be found in your IRAF/Gemini folder (probably a directory path similar to `~/iraf/gemini/gmos/data/`) or by typing `cd gmos$data`

<sup>3</sup>`sheila[at]physics[dot]unc[dot]edu`

in the IRAF/PyRAF environment. Reading the file into Python (example below) as a fits table reveals all the table columns: the fiber number (column name “NO”), x and y spatial position of each fiber in both arcseconds (“XINST”/“YINST”) and pixels (“XLDIS”/“YLDIS”), which block (bundles of 50 fibers) that the fiber is in (“BLOCK”), and whether the fiber is good or bad (“BEAM”).

Figure 1.1 shows the spatial positions of the fibers over an example galaxy on the top, while the bottom image shows the 2D information that is recorded on the CCD (wavelength on the x axis and fiber number on the y axis). This illustrates why we need the MDF to map the 2D image we get from the CCD to a 3D data cube of x and y position and wavelength later in the reduction.

The “BEAM” column tells us which fibers are good and bad (good fibers will have BEAM=1 while bad will have BEAM=-1). See Figure 3.3 for an example of what good/bad fibers look like and see § 4.3.1 for an example of why you may need to use/change this information.

## GMOS IFU Example Data: NGC 221

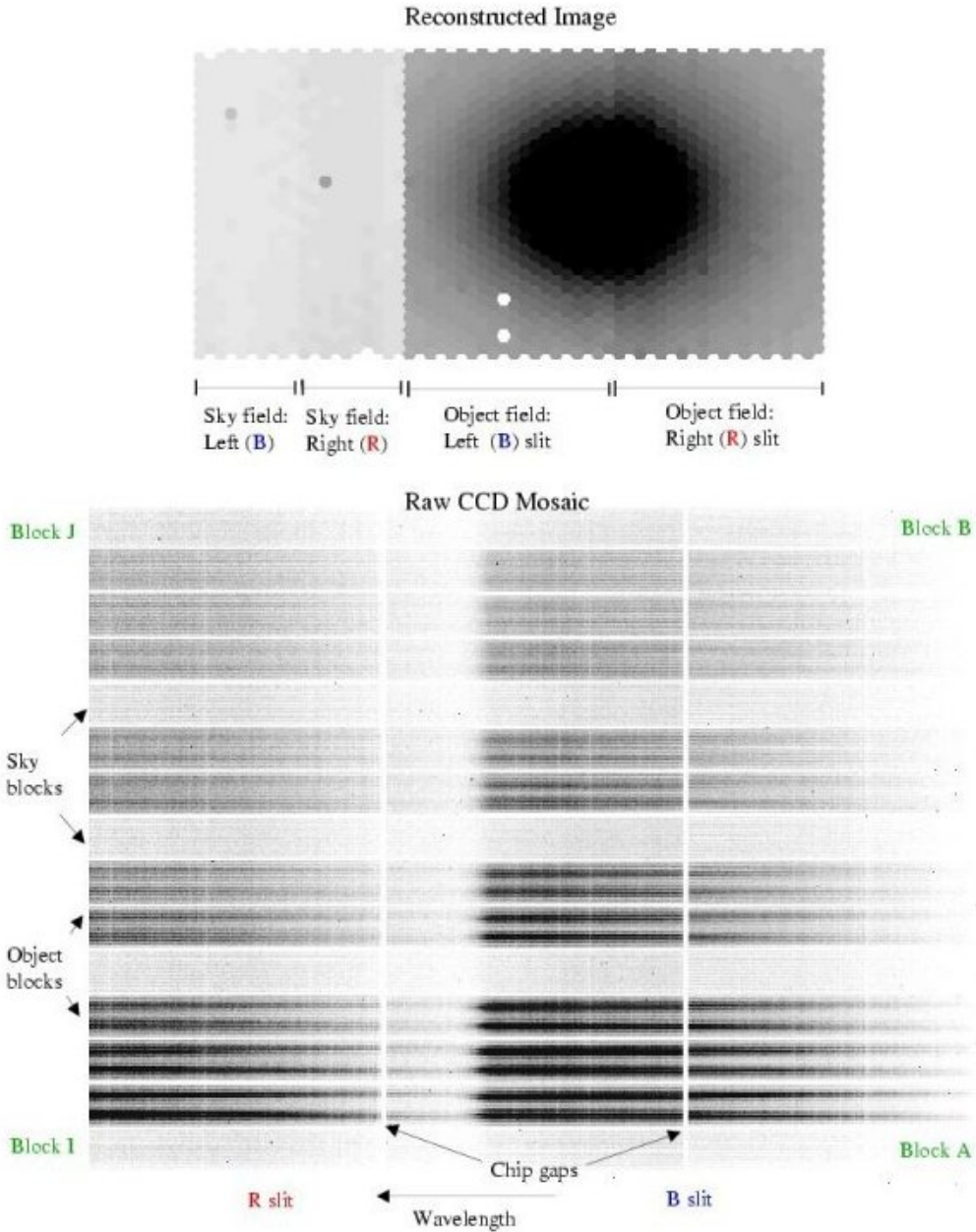


Figure 1.1: The top part of this image shows the IFU field of view over NGC221 (not a part of RESOLVE). The left portion of the image shows the sky spaxels, and the right portion shows the light of the galaxy. This is a 2D representation of the data we are getting – the third dimension is in the wavelength direction, and the darkness over where the galaxy is from summing the light inside each spaxel there. The bottom portion of this image shows the raw fits data from the above galaxies. Image from <https://www.gemini.edu/sciops/instruments/gmos/spectroscopy/integral-field-spectroscopy/field-slit-mapping>

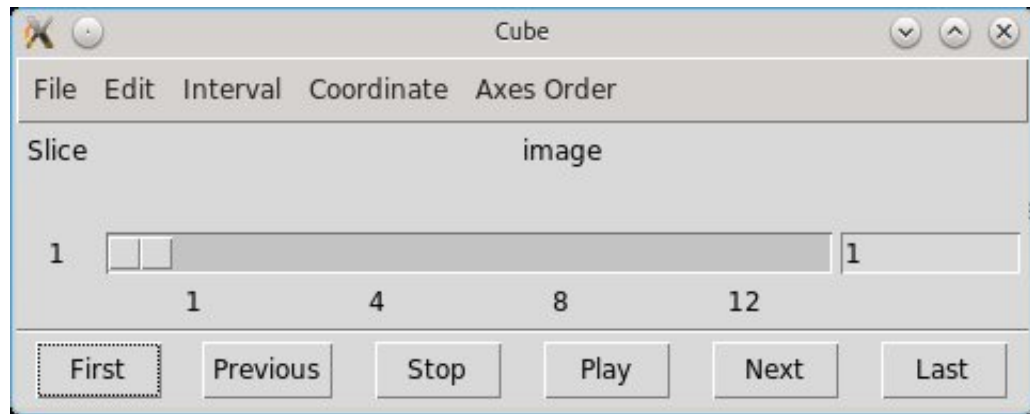


Figure 1.2: This is an example of the cube box that will open when you load a raw image in DS9.



Figure 1.3: This is an example raw image. Specifically this is a flat image, but you can also open the raw science and arcs. Each row you see is a fiber, and in the x direction is wavelength.

## Chapter 2

### Setting Up Your Workspace

There are some things you'll need to install (or update) before using this pipeline. The author highly recommends working in the Ureka environment, which includes easy-to-install versions of IRAF, Python, and PyRAF. Since this code is written for PyRAF, Ureka is indeed quite handy. Instructions on how to download Ureka can be found here: <http://ssb.stsci.edu/ureka/>. This pipeline was written and test using Ureka version 1.5.1 on cielo. Follow the instructions for making IRAF, and check your login screen to make sure it says you're using IRAF 2.16:

```
> pyraf
```

```
NOAO/IRAF PC-IRAF Revision 2.16 EXPORT Thu May 24 15:41:17 MST 2012
This is the EXPORT version of IRAF V2.16 supporting PC systems.
```

There is also an updated IRAF Gemini package you'll want to install. This version is not included in the Ureka download, but includes some updated tasks you will be using. Here's the link to this newest version as of February 2016: <https://www.gemini.edu/?q=node/11823>. You'll also want to check this when you're done by loading the 'gemini' package in IRAF:

```
--> gemini
```

```
+----- Gemini IRAF Package -----+
| Version 1.13.1, December 7, 2015 |
| Requires IRAF v2.14.1 or greater |
| Tested with Ureka IRAF v2.16   |
| Gemini Observatory, Hilo, Hawaii |
| Please use the help desk for submission of questions |
| http://www.gemini.edu/sciops/helpdesk/helpdeskIndex.html |
+-----+
```

This pipeline also makes use of a PyRAF script called PyFU which was written by James Turner, a support scientist at Gemini. The code will align and sum the data cubes we make during the reduction process. The package is available at the Gemini Data Reduction Forum (<http://drforum.gemini.edu/topic/pyfu-datacube-mosaicking-package/>), and comes with instructions on how to install and point to the package from your login.cl file.

You may also need to download L.A.Cosmic, an algorithm that finds and removes cosmic rays. You can read more about it at <http://www.astro.yale.edu/dokkum/lacosmic/>. You can download the IRAF spectroscopic version from that website, and will need to add a line in your login.cl: "task lacos\_spec = /path/to/where/you/put/it/lacos\_spec.cl". The pipeline will call this task during the cosmic ray removal step.

If you are new to data reduction in general, you will want to download DS9, an astronomical imaging application that you'll use to view our data as you progress through the pipeline. Download DS9 from this site: <http://ds9.si.edu/site/Home.html>.

You will now want to download the actual pipeline. You can access the code and this handy user guide at <https://github.com/emsnyder/geminiDRpipeline>. Always be on the lookout for updates in the future! You can place the code anywhere you like, but a nice folder structure would be to have individual folders for each galaxy with the pipeline code a level above.

Next, you'll want data to actually reduce. You should have flats, arcs, science frames, and a bias image (see § 4.1) before getting started. You should also have response flats from the baseline twilights and a flux calibration from the standard star data (§ 4.2 leads you there creation of these if you don't already have them). In § 1.4 there is more info on how to get your data and on each specific file you'll need. There should also be an observing log to inspect – your data package from Gemini should come with one, and for RESOLVE, they are called `obslog.txt` or just `log.txt`. The author has also created an alternative line list file called “`smalllinelist.dat`” that will be helpful during the wavelength calibration steps. This can be found in the `github` folder as the pipeline.

The current Gemini data are located on cielo at `/srv/two/sheila/emsnyder/gemini/data/`. From there, the folders are divided into different semesters: either 2013B, 2014B, or 2015B. In each of these folders, the galaxy data is further divided into individual folders titled the galaxy's name. Each of these folders should contain an observation log, raw flats, arcs, and science frames. There should also be folders for the baseline standards – usually these will be named `LTT####` or `H###`, after the stars we observed for our standard. These baselines may or may not be reduced already, and so if they are not, see § 4.2. If they are, just copy the needed files (usually named `*_resp.fits` for the response files and `sfunction_*.fits` for the flux calibration files) into your galaxy folder before starting. There should be two – one for both the red and blue setups. You can use the same baselines for each galaxy in that semester. There may also be a bias frame already in your galaxy folder, but if not, see § 4.1 for how to create one before getting started.

## Chapter 3

# Data Reduction Guide

### 3.1 How to Use This Guide

The author's goals for this user guide are threefold: to make it clear what you are doing in each step, to explain why each step is important and necessary, and to demonstrate how to successfully complete each step when user interaction is needed. Also included with each step is the name of the Gemini IRAF tasks being used, although the tasks are typically "under the hood" of the pipeline. For a more in depth look at what is going on, typing `help <name of task>` inside of PyRAF will open a detailed document with information about the task and what parameters you can change. This should make editing the task parameters in the pipeline easier, if it is ever needed.

### 3.2 Entering and Exiting the Pipeline

Here are the basic start up commands:

1. cd to the directory where you put your data
2. enter the Ureka environment by typing `ur_setup` in the command line
3. enter PyRAF by typing `pyraf` in the command line
4. enter the pipeline by typing `execfile('/path/to/your/code/gemreductionpipeline.py')`

To end your session:

1. type `CTRL-C` to exit the pipeline, if not out already
2. enter `.exit` to exit PyRAF
3. use `ur_forget` to exit the Ureka environment

### 3.3 Organizing and Identifying Your Data

The very first thing the pipeline does is ask you for the folder you are working in. Be sure to include the full path to your galaxy folder (including a trailing forward slash '/'), which can be found by typing `pwd` in your PyRAF window but outside of the pipeline. The pipeline checks that you are actually working inside this folder next, and will direct you to fix this if you are not. Next, it will ask if you are using a special MDF file (see § 4.3.1 for why this may be needed). If you are, be sure to give the full path to that file, and if not, just type `default`.

Next, the pipeline will ask if you are using a special MDF. If not, you can just enter `default` to use the standard file. The pipeline will then ask you if you have a bad pixel map already. If so, enter the path to the file, and if not, just enter `0` to create one later in § 3.7.

Lastly, the pipeline will look in your working folder and identify which files are there. It will print out the files it finds and whether they are arcs/flats/science/bias and which central wavelength they were observed at. It is good at this very first step to open up your raw images in DS9 to visually inspect your data files for any strange data. Also, be sure check the identifications against your observing log! Every file is identified by looking in the image headers, so problems here most likely will be missing images. If these all look correct, type `1` to go on, if not, press `0` which will exit the pipeline and let you figure out what's wrong/missing.

### 3.4 Bias + Overscan Subtraction and Trimming of the Flats and Fiber Identification

Gemini IRAF task used: `gfreduce`

This very first step can often (in the author’s experience) be the most time-consuming step of the entire reduction. We use the flats not only for flat fielding the science data, but also to correctly order the fibers in the raw data. See bottom of Figure 1.1 – each row is an individual fiber spectrum that must be correctly numbered, which ensures that we can successfully map our raw 2D data to a 3D (x, y, wavelength) data cube. The IRAF task `gfreduce` has many different options, but for this very first step, we are just going to attach the MDF file, do a bias subtraction, overscan subtraction, image trimming, and fiber ID so that we may extract all the spectra. We will later re-extract the flats after performing a quantum efficiency correction, but we need to identify the fibers and ensure our MDF is correct before attaching it to other files.

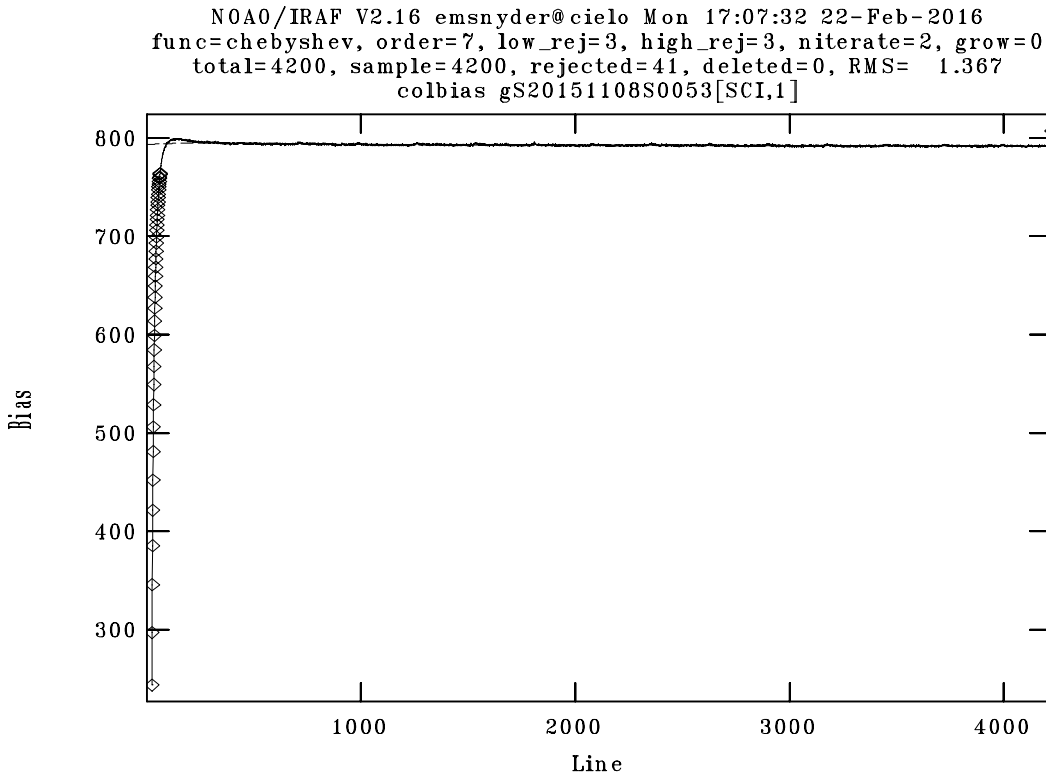


Figure 3.1: An example of the overscan subtraction window that PyRAF will open during the reduction of the flats step. The solid line represents the data, while the dashed line shows the fit to that data. The diamonds are data points that are being rejected from our fit.

1. The MDF attachment is done without user input needed. Corresponding to each input flat file, a new file is created in your working directory with the prefix ‘g’. A useful way to remember this could be “g” is for “Get the MDF”
2. The bias and overscan subtraction and imaging trimming is mostly done without user input needed. The overscan regions are the regions of the image with no data, i.e., between the chips and amplifiers. We want to measure the count level in these regions and then trim them from our images. Note that we also trim the outer edges of the image where there is no data in this step too, but we are not measuring the counts there for the overscan subtraction. To do this, a PyRAF window will open with the overscan level being plotted. Also plotted is a best fit line to the

overscan level, and this normally looks fine as is. Press `q` inside the PyRAF window to move on. There is a plot for each amplifier in the CCDs, so you will see 12 individual plots. If the fit does not look fine, you can type `:order #` and then `f` inside the PyRAF window to change the order of the fit to a different number (with that number instead of `#` in the previous command). Higher orders typically do better at fitting any strange features (spikes/dips). Unless something is very wrong, you probably won't need to worry about this. See [Figure 3.1](#) for an example of what you should be seeing. This step produces a file with the prefix “rg”, where the “g” comes from the previous step and the “r” is added for the “subtRaction/tRimming” (this one is a stretch – sorry).

3. Lastly, we must tackle the fiber identification. Your command window is going to ask you a few questions:

`Extracting slit 1`

`Find apertures for ergS20151108S0053_1? ('yes')`:

Here I recommend saying ‘yes’, as usually IRAF will be able to identify the fibers correctly for you.

`Edit apertures for ergS20151108S0053_1? ('yes')`:

Say ‘yes’ to this one as well, so we can inspect the fiber IDs and make sure everything looks correct. The left side of [Figure 3.2](#) shows what this will look like – a complete mess! But we can zoom in by typing `w` in the PyRAF window, and then typing `e` at the bottom-left of the first “fiber bundle” and again at its top-right. [Note: use `w` and `a` to un-zoom the window.] You should now have a screen that looks like the right side of [Figure 3.2](#). I find that making this plot full-screen helps immensely. Each ‘bundle’ contains a set of 50 fibers, which you will see numbered at the top of your screen (these are hard to see in [Figure 3.2](#)). Your job is to make sure each fiber is identified correctly – this means no fiber is identified twice, and any bad fiber numbers are skipped (not used) in the numbering. The fibers should be numbered from 1-750 or 1500, from left to right. Often I find that the low level of fiber 50 makes it get skipped in IRAF’s auto-finding scheme, which makes the first fiber of the second ‘bundle’ start at 50 instead of 51. If this happens, you can use `d` in the plot window to delete the IDs for fibers 50–750, and then use `m` to re-mark the fibers including the low-level fiber. This is where it can get time-consuming.

Figure [Figure 3.3](#) shows an example of a bad fiber not being marked in the identification process. This is exactly what we want to happen in this case. If, for example, fiber 138 was still “on”, you would want to edit the MDF to turn it “off” (i.e., set BEAM=-1 for that fiber number). See [§ 4.3.1](#) for how to do this, and for more info on how this step can go wrong. For the 2014-2015B slit-1 data, you will end with either fiber 742 or 743, depending on how the telescope was rotated at the time of the observation.

If you are pleased with your IDs, type `q`. More questions will appear in the terminal, but it will want your answer inside the PyRAF graphics window.

`Trace apertures for ergS20151108S0053_1?`

`yes`

`Fit traced positions for ergS20151108S0053_1 interactively?`

`NO` (the capitals will tell IRAF no to all)

`Write apertures for ergS20151108S0053_1 to database`

`yes`

`Extract aperture spectra for ergS20151108S0053_1?`

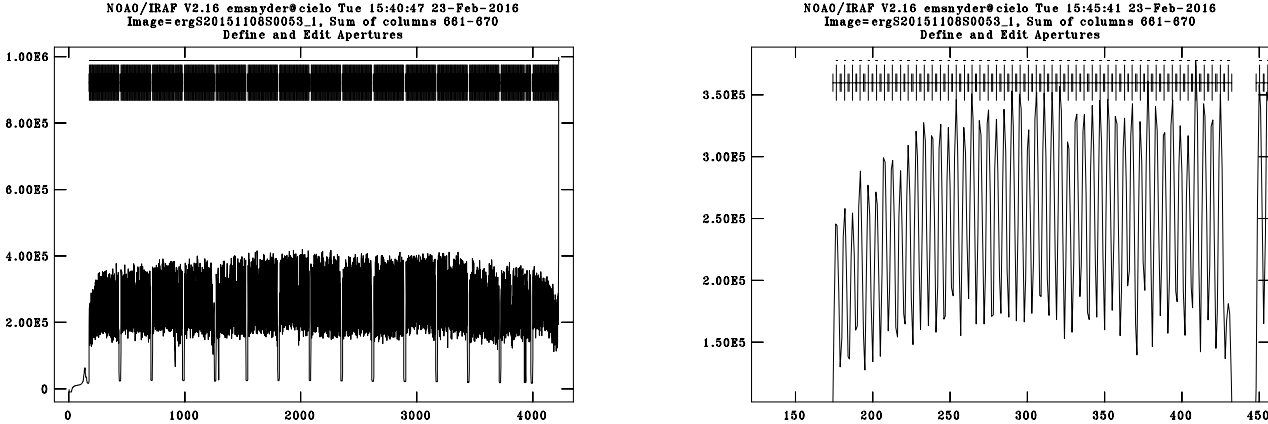


Figure 3.2: (a). A zoomed-out example of the fiber ID window that PyRAF will open during the reduction of the flats step. The numbers above each fiber are blurred together here. (b). An example of the fiber ID window that is zoomed-in on one set of fiber bundles. The numbers for each fiber aren't visible in this example but will be above the aperture marks at the top.

**yes**

Review extracted spectra from ergS20151108S0053\_1?

**NO**

If you're in the blue setup (1-slit mode), this is the end of IDing for you! If you're in the red setup (2-slit mode), you'll have to repeat this process for fibers 751–1500 (usually fibers 1493 and above are missing for this group). Once complete, IRAF will extract all the spectra and create a file with the prefix “e” (for “Extracted”), so in full you should have an ‘ergS....fits’ file in your working directory. Extracting takes out the sky spectra, reorders the science spectra, and arranges them by slit. This means our output files will go from having 12 extensions to having only one or two, depending on whether you're working with 1- or 2-slit data. Since we have two different wavelength dithers, you'll have to repeat this process for the second flat, but after that, we'll use these “erg” flat files to identify the fibers for the rest of the files (including the arcs and science).

### 3.5 Overscan Subtraction and Trimming of the Arcs

Gemini IRAF task used: `gfreduce`

Just as for the flats, we now attach the MDF file, do an overscan subtraction, and trim the arcs. We do not perform a bias subtraction on the arcs because they are read out from the CCD faster than our other data, meaning the read noise for them will be different than what's in our bias frame. We still do the overscan subtraction as a rough estimate of the bias level to subtract and we don't worry about any bias structure, which should be irrelevant if the arc lines are strong. Therefore, there is nothing interactive for this step. New files will be created with the prefix “rg” in your working directory (they are not yet extracted).

### 3.6 Bias + Overscan Subtraction and Trimming of Science Data

Gemini IRAF task used: `gfreduce`

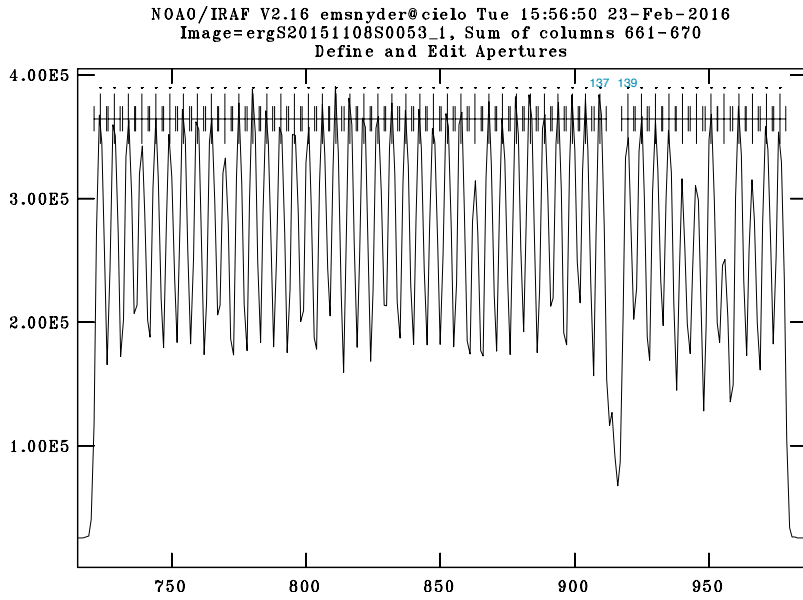


Figure 3.3: For this image, fiber 138 is bad. However, the MDF shows that BEAM = -1 for this fiber number, and thus that number is skipped during the identification routine.

Next, we perform the bias and overscan subtraction and trimming of the science frames. Nothing interactive is needed here, but again files will be made with the prefix “rg”.

### 3.7 Identification and Removal of Bad Pixels from the Science, Flats, and Arcs

Gemini IRAF tasks used: `addbpmp` and `gemfix`

The pipeline prompted you at startup to enter the name of a bad pixel map (BPM) file. If you didn’t give a file at the prompt, read on and you will be lead through what a BPM is and how the pipeline will help you make one.

Before we get too far into the reduction, we must look at one of the bias- and overscane-subtracted and trimmed science images (aka, the “rg” file made in § 3.6) and find any hot pixels or bad columns on the CCD itself that could later affect the reduction. The bad pixels are usually different for images taken with different exposure times since bleeding can occur, so we’ll create a BPM for the science frames only since they have the longest exposure time. We also look at the bias frame itself, since any hot pixels should stand out better in it than in the science frames since cosmic rays will be everywhere in the science. A BPM is a fits image that has the same dimensions and number of extensions as the science image, but the pixel values are only zeros and ones. The zeros denote where the pixels are good, and the ones flag where the pixels are bad. A useful caveat to bad pixels or columns on a CCD is that they will normally not change quickly, so it is okay to flag the same pixels for data sets taken in the same semester. So, if you’ve already created a BPM for a galaxy in the same semester, you can enter its name at the pipeline prompt to use it. If this is your first galaxy of the semester, the pipeline will now lead you through how to make one.

The pipeline starts by creating an image of the correct size that’s entirely made of zeros. Now, we must identify the bad pixels in our science and bias images, making note of their x and y positions and which extension they are on. The pipeline will open a DS9 window with one of the science frames (the “rg” file made in § 3.6) and the bias frame. The pipeline will then prompt you to look through all twelve extensions and identify any bad pixels or columns you see. If you don’t see any bad pixels, you can enter `0` and move on to the arcs. If you do see some bad areas, enter `1`, which will bring up

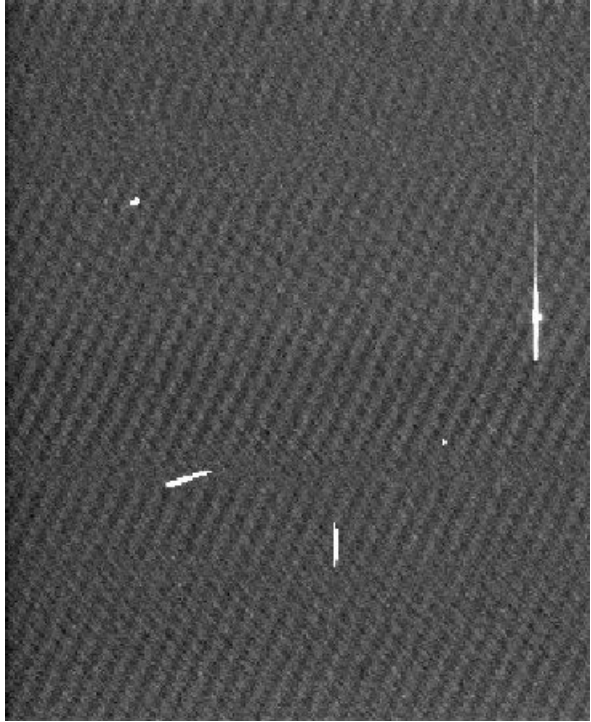


Figure 3.4: This shows you both cosmic rays and bad pixels in one of the science frames.. The long line on the right side is a bad column, whereas the other four bright spots are probably cosmic rays. These are not “bad pixels” because they change in every image.

another prompt for you to enter the extension number, and x and y values of the bad region. The extension number can be 1-12, and x and y can extend to the full size of your image. To enter a bad rectangle, you can say  $x = 132:140$  and  $y = 444:450$ . For a full column, you can enter \* for y.

It is important to discern between cosmic rays and bad pixels/columns too. The author usually finds that cosmic rays will be curved and erratic looking, while actual bad columns will be in straight lines and may be much larger, although the extent varies so single hot pixels are also possible. See § 3.7 for an example. Generally, you’ll have the same bad areas in all of your images, but the extent of the damage due to these pixels can vary due to exposure time. So, if you’re unsure of bad pixels vs. a cosmic ray, look in the other images to see if there are bad pixels in the same spot.

After feeding the pipeline the coordinates of the bad pixels, it will change the BPM values to 1 from 0 at those locations. We then use the task `addbpm` to attach the BPM to our data file, so that `gemfix` can find it and interpolate over the bad pixels. The pipeline will then use this BPM to correct the science, arc, and flat frames.

Note that in this step we are applying this correction to the images with prefixes “rg”. This step adds the letter “p” for “fixing Pixels”.

### 3.8 Extraction of the Arcs

Gemini IRAF task used: `gfextract`

We now extract the spectra from the BPM-corrected arc images using the fiber IDs that were created from the flats. There is nothing interactive to be done, but file will be made with an “e” in front for the extracted arc spectra (the full prefix is now “eprg”).

### 3.9 Creation of the Wavelength Solution

Gemini IRAF task used: `gswavelength`

Next, the pipeline calls `gswavelength` and a PyRAF window will open with an image that looks like [Figure 3.5](#). This is a 1D spectrum of the arc lamp, and we'll use it to assign a wavelength to each pixel for our science data (this is called a “wavelength solution”). You should see that some of the emission lines are being automatically marked with | above them.

A quick aside about the lines being automatically ID'd: if you aren't using the “smalllinelist.dat” that was included in the download of the pipeline or if it isn't in your working directory, the pipeline will use the default line list from Gemini, which is called `GCALcuar.dat` and is located in the `gmos$data` directory (something similar to `~/iraf/gemini/gmos/data/` outside the PyRAF environment). The difference between these two lists is that the author has taken the strongest lines from the default list and placed them into “smalllinelist.dat”. Using this list with the strongest lines only should save you time as you perform each fit since these weak lines would most likely need to be deleted anyways. When using “smalllinelist.dat” you should see only  $\sim 10$  lines identified automatically.

Press `f` to see the fit residuals, which should look something like [Figure 3.6](#). The number to pay attention to here is the RMS. I try to keep this under  $\sim 0.09\text{\AA}$ , which, after some experimenting, I've found produces a good wavelength solution. To delete bad points, type `d` and then press `f` to refit. The RMS should update after pressing `f`. You can also change the order of the fit using `order: #` and then `f`. The default order is 4, which seems to work well most of the time.

At times, especially when going from slit 1 to slit 2, the first line on the left will be misidentified. You can delete lines with `d` and then re-identify them by hovering your mouse above the correct line, typing `m`, and then entering the correct wavelength (see [Figure 3.5](#)). Refitting with `f` should then yield a better RMS value.

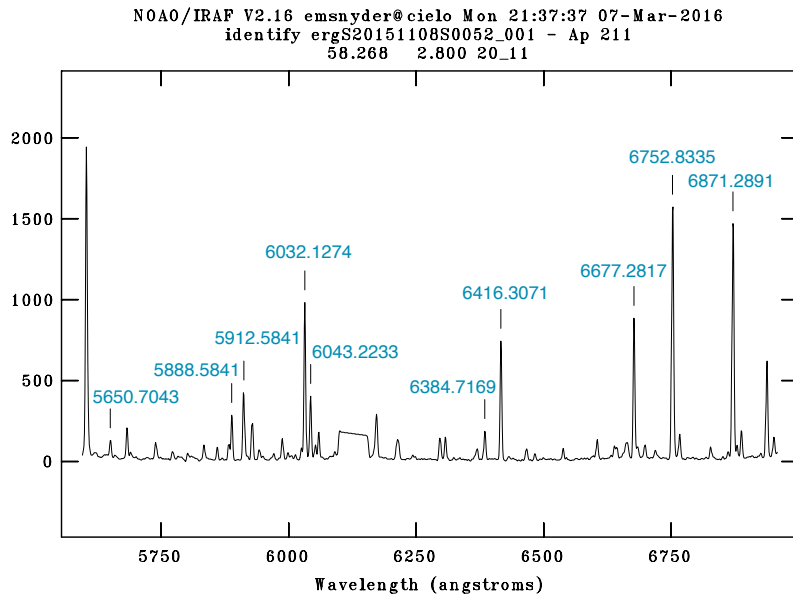


Figure 3.5: This image shows an arc spectrum. The arc lamps have certain unchanging emission lines, by knowing the wavelengths of those lines we can create a function that assigns a wavelength to each of our image pixels.

You will see on your PyRAF screen some text that looks like this:

Image Data	Found	Fit	Pix Shift	User Shift	Z Shift	RMS
------------	-------	-----	-----------	------------	---------	-----

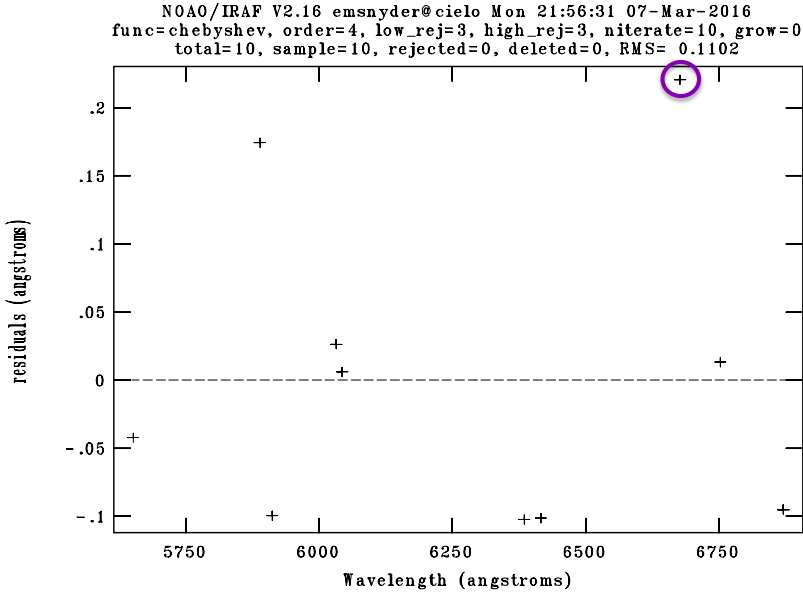


Figure 3.6: This image shows the residuals of the wavelength function fit. To improve this fit, I would delete, using `d`, the circled point. You can also change the order of the fit if the default (4) doesn't fit well enough by typing `order #` and then pressing `f` again.

```
ergS20151108S0106_001 - Ap 440 10/10 10/10 -0.00557 0.00522 1.82E-6 0.0749
Fit dispersion function interactively? (no|yes|NO|YES) ('no'):
ergS20151108S0106_001 - Ap 441 10/10 10/10 -0.0793 0.081 1.36E-5 0.0731
Fit dispersion function interactively? (no|yes|NO|YES) ('no'):
ergS20151108S0106_001 - Ap 442 10/10 10/10 -0.0694 0.0711 1.12E-5 0.034
Fit dispersion function interactively? (no|yes|NO|YES) ('no'):
ergS20151108S0106_001 - Ap 443 10/10 10/10 -0.00833 0.00873 9.11E-7 0.0476
Fit dispersion function interactively? (no|yes|NO|YES) ('no'):
ergS20151108S0106_001 - Ap 444 10/10 10/10 0.0222 -0.0225 -4.0E-6 0.07
Fit dispersion function interactively? (no|yes|NO|YES) ('no'):
ergS20151108S0106_001 - Ap 445 10/10 10/10 0.0256 -0.0259 -4.7E-6 0.0896
Fit dispersion function interactively? (no|yes|NO|YES) ('no'):
ergS20151108S0106_001 - Ap 446 10/10 10/10 0.084 -0.0855 -1.4E-5 0.126
Fit dispersion function interactively? (no|yes|NO|YES) ('no'): yes
```

My way of conquering this task is to answer `no` to each prompt until I see an RMS value that needs attention. For example, the last row in the above text is where I said yes to fit the wavelength function interactively when the RMS was 0.126. If the RMS is okay, I won't fit it interactively. You will need to do this for each fiber in each arc (usually just two per galaxy). The outputs for this step are files in the database named "idergS....\_001" and "\_002" (if in 2-slit mode).

### 3.10 Application of the Calibration to the Arcs

Gemini IRAF task used: `gftransform`

This step simply applies the wavelength solution you just found to the arc lamps itself. A good way to check our work here is to make sure the arc lines in the output image (which will start with the prefix "t" for "Transformed") are straight, as opposed to curved. See Figure 3.7 for a before and after. The pipeline will open a DS9 window with the transformed arcs so that you can check for any

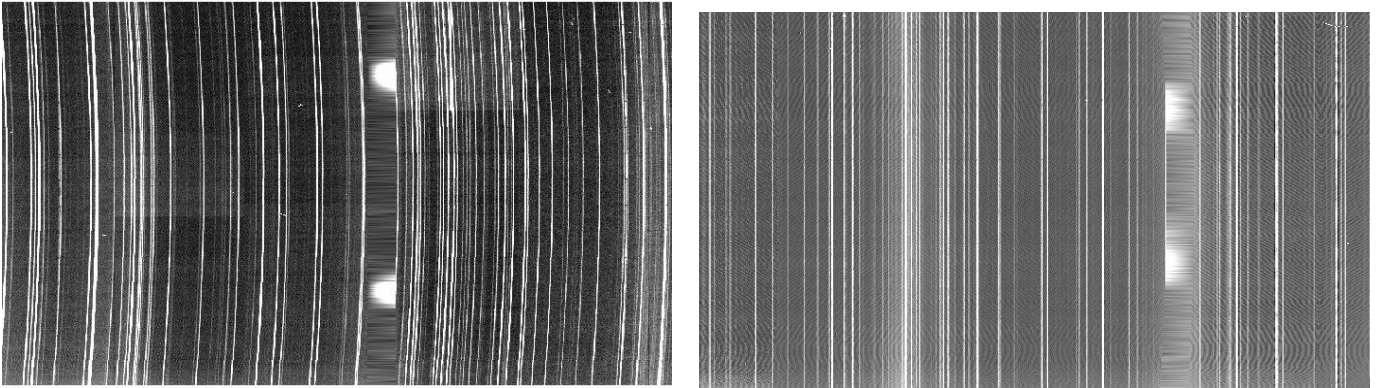


Figure 3.7: A DS9 view of the arc (a.) before and (b.) after the wavelength transformation has been applied.

errors. If everything looks good, we can move on. See § 4.3.2 for an example of a bad wavelength transformation and for information on how to correct issues or start over if needed.

### 3.11 Quantum Efficiency Correction of the Flats

Gemini IRAF task used: `gqecorr`

Some CCDs will have different quantum efficiency levels between CCD sections or amplifiers, so this step corrects for this effect. The file used for these corrections is in `gmos$data` (like the MDF) and is called `gmosQEfactors.dat`. Nothing interactive is required. This step creates files with the prefix “q” for “Quantum efficiency corrected”.

### 3.12 Re-extraction of the Flats

Gemini IRAF task used: `gfextract`

Now the flat spectra will be re-extracted, using the same fiber IDs as before, but this time pulling out the BPM- and QE-corrected spectra. Again, nothing interactive must be done. After this step, our flats will have the prefix “eqprg”. The flat images with prefixes “erg” will no longer be used from now on.

### 3.13 Creation of the Response Functions

Gemini IRAF task used: `gfresponse`

Next, we use the twilight flats from our baseline standard data and our newly extracted flats from § 3.12 to create a response function to use for flat fielding the arcs and science data. This response function takes into account three difference effects: pixel-to-pixel variations in the CCD itself, the wavelength-dependent pixel efficiency (i.e., pixels being more responsive to blue light than red light), and illumination variations (corrected using the twilight flats). There is nothing interactive for this step, and the output will be named “eqprgS....resp.fits”. See § 4.2 if you need to make your twilight flats.

### 3.14 Quantum Efficiency Correction of the Arcs

Gemini IRAF task used: `gqecorr`

We now correct for the quantum efficiency differences in the arc images, as we did for the flats in § 3.11. Again, nothing interactive is required.

### 3.15 Flat Fielding and Extraction of the Arcs

Gemini IRAF task used: `gfreduce`

And now we use the response functions made from the twilights to flat field the arcs, and then re-extract them. Nothing interactive is needed for this step, and a file with the prefix “e” is made.

### 3.16 Re-creation of the Wavelength Solution for the QE-Corrected & Flat Fielded Arcs

Since the QE correction and flat fielding can change the pixel values in the arcs, we now need to redo our wavelength solution for the arcs. The steps will be the same as in § 3.9. The reason we must do this twice is because we need a wavelength solution in order to perform the QE correction. Future work may include finding a way to automate these wavelength solution steps.

### 3.17 Application of the Calibration to the QE-corrected & Flat Fielded Arcs

Gemini IRAF task used: `gftransform`

Again, we must apply the new wavelength solutions to the QE-corrected and flat fielded arcs. The pipeline will open the transformed arcs so that you may check for a good solution.

### 3.18 Cosmic Ray Rejection in the Science Data

Gemini IRAF task used: `gemcrspec`

Next, we use L.A. Cosmic to find and remove cosmic rays from our science spectra. The code will iterate many times, and may take a few minutes to complete. Nothing interactive is required, and a file with the prefix “x” is created for “eXpunge cosmic rays”.

### 3.19 QE Correction of Science

Gemini IRAF task used: `gqecorr`

We now QE correct the science frames, as we did for the flats and arcs in § 3.11 and § 3.14. Again, nothing interactive is needed here, and you should have files made with the prefixes “qxprg”.

### 3.20 Flat Fielding and Extraction of Science

Gemini IRAF task used: `gfreduce`

Next, we use the response functions made from the twilights to flat field our science data, and then extract it. Nothing interactive is needed here, and a file with the prefix “e” is made.

### 3.21 Wavelength Calibration of Science

Gemini IRAF task used: `gftransform`

In this step, we apply the wavelength solution we found in § 3.16 to the science frames. There is nothing interactive for this step, and file is created with the prefix “t”.

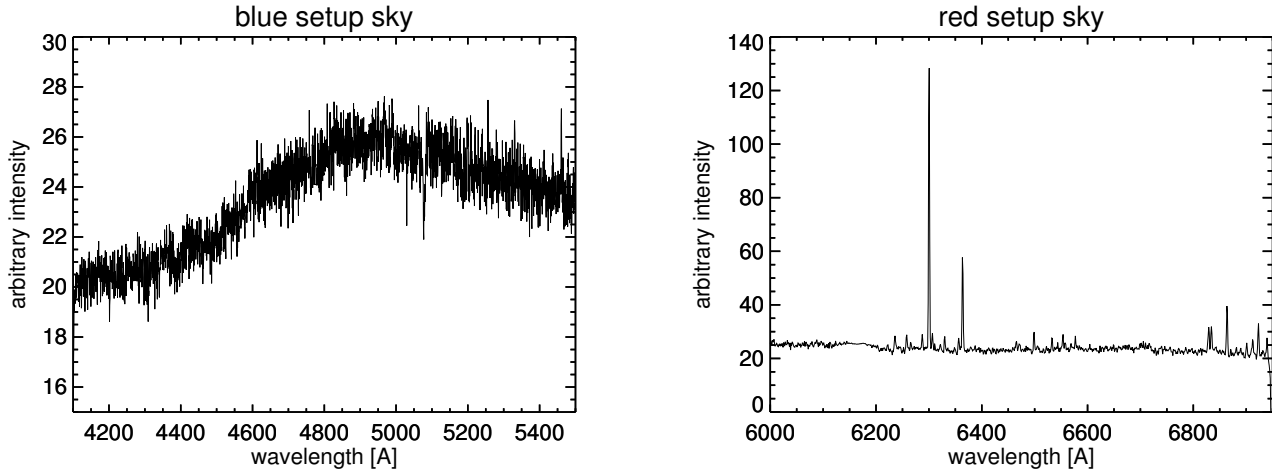


Figure 3.8: An example of the sky spectrum for (a) the blue setup data and (b) the red setup data. The blue setup data has no large sky lines, but this could vary depending on moon phase and cloud coverage during your observations. RESOLVE typically will not observe blue setup data when the moon is bright or weather is poor, so sky lines in the blue setup are rare.

### 3.22 Sky Subtraction of Science

Gemini IRAF task used: `gfskysub`

Now, we can pull out the spectra of the sky fibers and use them to subtract the scattered sky light and sky lines from the science spectra. This step is done non-interactively, but the basic process is that the task will take the median of all the sky spectra and subtract that from our science spectra. Doing a median of the spectra will ensure no spurious peaks from poorly removed cosmic rays will affect the subtraction. A file with the prefix “s” is made here for “Sky subtracted”. The sky spectrum is appended to this newly made file under extension 2 or 3<sup>1</sup>. You can plot this spectrum in IRAF with `splot` outside of the pipeline, or load it into python. You should see spectra similar to those in Figure 3.8 for the blue setup (on the right) and the red setup (on the left). Also note that the intensity of sky lines may vary due to moon phase or cloud cover, so yours may look slightly different.

### 3.23 Flux Calibration of Science

Gemini IRAF task used: `gscalibrate`

The second to last step of the reduction uses the flux responses from the standard star data to flux calibrate our science data. Nothing interactive is needed here, and a file with the prefix “c” for “Calibrate flux” is created. If you do not have flux responses, see § 4.2 for how to make them.

### 3.24 Data Cube Creation

Gemini IRAF task used: `gfcube`

Now that we’re nearing the end of the reduction process, we resample our spectra into data cubes. The pipeline will sample the data into 0.2” pixels, since that’s the size of the fiber and will make the

<sup>1</sup>Extension 0 is the MDF, 1 is the first slit, 2 is the second slit if in red setup, or the sky if in blue setup, and 3 will be the sky for the red setup

next step (applying RA/Dec coordinates to each pixel) easier. There will be as many data cubes as there are science images, meaning the spectra taken at different wavelength dithers or at different spatial positions are not yet merged. We use the task `gfcube map` the 2D images into 3D data cubes using the information from the MDF and our fiber IDs. See § 4.3.1 if you get an error here. Files with the prefix “d” are created here for “Data cube”. You can open these outside the pipeline in DS9 and will get a 2D image in x and y with a dialog box that lets you “scroll” through the wavelength axis. You should be able to see in the blue setup data some continuum light, but most likely not much for the red setup, until you get to the wavelength of H $\alpha$ , where you should see tons of emission!

### 3.25 Creation of a WCS Solution

Next the pipeline will assign a coordinate system to the individual cubes. This RA/Dec coordinate system is called a world coordinate system (WCS) solution. Data cubes taken in the same position but with different wavelength dithers will have the same WCS solution, but data cubes taken at different spatial offsets will have different ones.

To do this, we start by getting the information in the headers of the last acquisition image, which will provide us with starting WCS. There will be CRPIX1 and CRPIX2 that give the reference x and y pixels, along with CRVAL1 and CRVAL2 that are the RA and Dec values at the reference coordinates. The pipeline then calculates the central x and y pixels of that image (i.e., the size of the image in the x and y directions, divided by two.) Now we need to account for the offset from the telescope pointing position to the IFU field of view, since the FOV isn’t centered. Thanks to the Gemini-South data reduction gurus James Turner and German Gimeno, we have these offsets and the pipeline calculates the center pixels of the IFU by subtracting these offsets from the central x and y pixels of the acquisition image. We can then use the starting WCS to convert these pixels values into RA and Dec coordinates.

Now that we know the RA and Dec of the center of the IFU FOV, we can assign those coordinates to the center x, y pixel of the data cube. Knowing that each pixel is 0.2” in diameter and the PA at which the observation was taken, the pipeline calculates the RA and Dec for every other x,y pixel in the data cube. It lastly puts this information in the image header, so that the next step can find it.

### 3.26 Summation of the Data Cubes

Now that the data cubes have image headers with accurate WCS coordinates, we can use the tasks included in the PyFU package to mosaic the cubes together. The Python script `pyfmosaic` looks into the headers of the supplied input data cubes and pulls out both the WCS information and the spectral offsets. Each individual cube may have slightly different spectral resolution ( $\text{\AA}$  per pixel) since we created the wavelength solution for them separately, so PyFU will rebin the spectra to the same resolution and then sum each pixel in the spectra in the different cubes according to their spectral dithers. See ?? for a sketch of this process. Once the dithers are combined, PyFU will combine the spatial offsets using the WCS solutions from the image headers. The product is one final data cube, named `yourgalaxyname_final.fits`. The data reduction is complete!

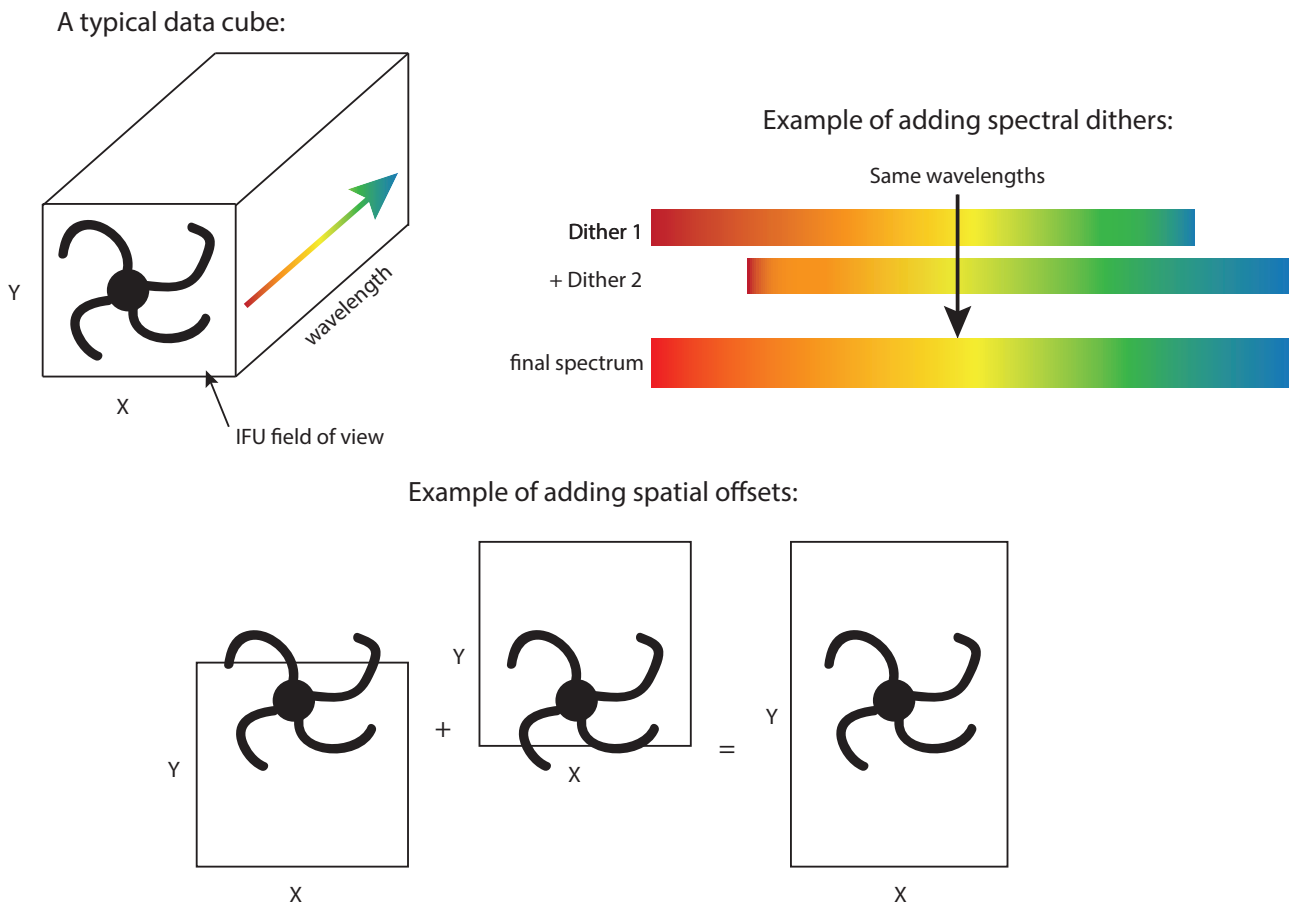


Figure 3.9: In this image, we show an example schematic of a data cube, and then examples of how the spectral dithers and spatial offsets are combined.

## Chapter 4

# Other Things You’ll Want to Know

## 4.1 Creating the Bias Frame

Before starting the reduction, you’ll want to make sure you have bias frame made, or individual biases that we can combine to make the bias frame. Each night after observing is complete, a standard set of bias frames are observed by the Gemini South operators. They are a little tricky to find in the Gemini Science Archive online database, but you can go to the “View Associated Calibrations” tab to find all of the biases taken for your observing program. Usually, searching on the observation date, the correct binning (CCDSUM 2 1), and the correct filter (see [Table 1.1](#)) will yield 5 bias frames to download and process with the Gemini IRAF routine, `gbias`.

Outside of PyRAF, first download the frames from the database. These will come in tar file, and you can use `tar -xvf gemini_data.tar` to untar the files. The individual files are “bzipped” with the extension .bz2. Type `bunzip2 *.bz2` to unzip the files.

Now, enter PyRAF and type `gemini` and press enter, and then type `gmos` and press enter again. This loads the packages needed to access the task `gbias`. Now type `epar gbias` to open the PyRAF parameter editor. You should see a separate window open with Task = GBIAS at the top. Fill in the following boxes/checkmarks:

```
inimages = bias1.fits, bias2.fits, bias3.fits, bias4.fits, bias5.fits
outbias = <date>bias.fits
fl_over = yes
fl_trim = yes
```

Note that for `inimages` you can use wildcards, so for the biases taken on night Nov 11, 2015, you could also put `S20151111*.fits`, assuming you are working in a separate folder with no other files from that night in there. You can also name the output file (`outbias`) whatever you like, as long as it has the word “bias” in it since this is what the pipeline searches for. The author usually names hers with the observation date followed by “bias”.

Then press `Execute` at the top of the dialog box to run the task. If everything runs smoothly, a bias frame will be output. Open this in DS9 to make sure it looks good. See [Figure 4.1](#) for an example.

The author also notes that since the flats, arcs, and science are all overscan subtracted and trimmed via the pipeline, the bias frame should be as well. You will get an error if your bias doesn’t match the format of the flats/arcs/science! If for some reason you want to forego overscan subtracting and trimming, you will need to manually edit the pipeline to turn those features off.

## 4.2 Reducing the Twilight and Standard Star Data

The reduction process for the baseline standards is extremely similar to the process described above for the galaxy data, with a few added steps at the end. Here is a step-by-step primer of the changes:

1. Start up will be the same as in [§ 3.2](#), except that you will instead load the file “gemstandard-pipeline.py”.

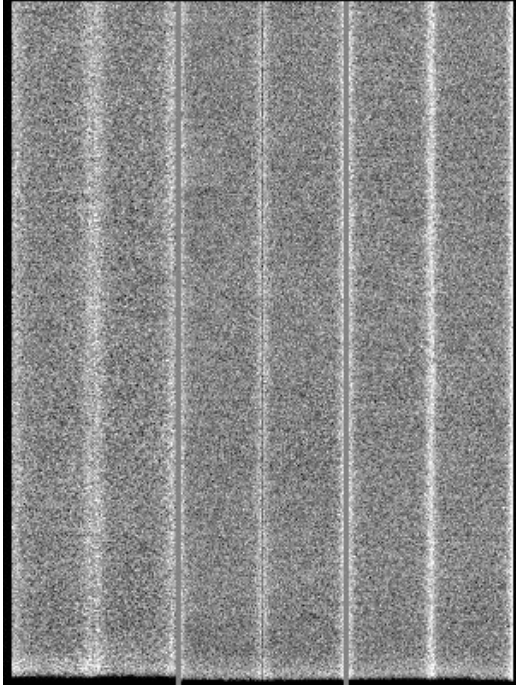


Figure 4.1: Example of the bias frame taken on the night of November 10, 2015. The near the edges of each amplifier in the CCD, the bias level rises.

2. The pipeline will ask you for your working directory, the standard star's name, it's shortened name, the MDF file, and BPM. The star name will probably be either LTT#### or H###, and this can be found in your log. The shortened name is for the LTT stars only, since the pipeline will search for its calibration data using the name L####. Everything is the same as in § 3.3. It will again print out the files it finds in your working folder, and you should be arcs, flats, science (this time a star instead of a galaxy), and also twilight flats.
3. Then the pipeline will take you through the bias/overscan subtraction, trimming, and fiber ID for the flats, just like in § 3.4.
4. It will then overscan subtract and trim the arcs, and bias/overscan subtract and trim both the science frames and twilight flats. These are detailed in § 3.5 and § 3.6. The twilights will be treated much like regular flats throughout this reduction.
5. Next the pipeline will either perform the BPM correction if you already have a BPM file made, or will lead you through how to make one. Details on this are in § 3.7.
6. Then the arcs are extracted (§ 3.8), and you will create the wavelength solution (§ 3.9), and apply the transformation (§ 3.10).
7. The pipeline then will quantum efficiency correct (§ 3.11) and re-extract (§ 3.12) the flats.
8. The pipeline now repeats the above step for the twilight flats. **These are the two files (one for both wavelength dithers) you will need to copy over to your galaxy directory to make the response functions for flat fielding.** They will be have the prefix “eqprg”, but you may need to look in your log to find the correct file name base (for example, S2014....fits).
9. Next the response function is create for later flat fielding our standard star data. This process is detailed in § 3.13.
10. Now the pipeline quantum efficiency corrects (§ 3.14) and flat fields (§ 3.15) the arcs and leads you through remaking the wavelength solution (§ 3.16) and transformation (§ 3.17).
11. We now move on to the standard star science data. The cosmic ray rejection is first (detailed in § 3.18) and then quantum efficiency correction occurs (§ 3.19).
12. Then the pipeline flat fields and extracts the science spectra using the response function from step

9. This is detailed more in § 3.20.
13. Next the science frames are wavelength transformed (§ 3.21) using the output of step 10, and then sky subtraction occurs (§ 3.22).
14. The pipeline now sums the light in all the fibers to create a 1D spectrum for the standard star. Then, it creates the sensitivity curve files using the task `gsstandard` using the ID spectrum just made as the input file. The task will output two different files: “`sfile_steqxprgS...`” which is a text file that contains the output fluxes from the star and “`sfunction_steqxprgS....fits`” which is a fits file that contains the sensitivity function. The routine compares the known fluxes of the standard star you observed to the observed values to create the sensitivity function. **The two “`sfunction....fits`” files will need to be copied over to your galaxy directory for the flux calibration step.**
15. We can check our work by flux calibrating the standard star itself. This process is explained in § 3.23.
16. Lastly, data cubes are made for the standard star, and the reduction is complete! Be sure to check the data cubes to make sure everything looks normal. You can use the same twilight files and sensitivity functions for each galaxy observed the same semester as the standard.

## 4.3 When Things Go Wrong...

### 4.3.1 A Bad Fiber Identification

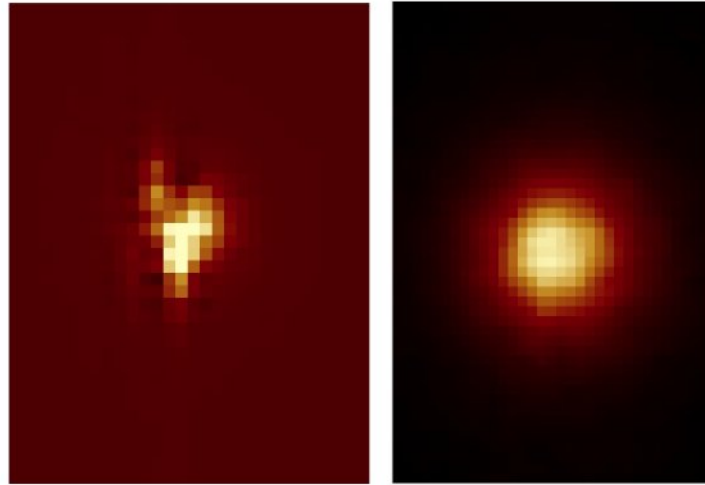


Figure 4.2: On the left is an image of a standard star that has been incorrectly reconstructed in DS9 due to the fibers being improperly identified. On the right is an image of how the star will look with the correct IDs applied. Image is Figure A.2 from <http://arxiv.org/abs/1409.8264>.

There are two ways (that the author is aware of) to discover that the fiber ID step has gone wrong. First, the shape of your object will look just plain wrong! After creating data cubes of your science data, you can open them in DS9 and check to make sure the object looks like it should. Figure 4.2 shows this for standard star data. Second, you may not be able to make a data cube at all. If you have ID'd more fibers than are turned on in the MDF, you will get an error from the task `gfcube` saying “number of apertures identified does not equal the number of apertures defined in the MDF”. Sadly, you won't be able to test your IDs until making the data cubes, and so you may need to start from scratch.

To correct the first issue, start by removing the IDs that are located in your database directory. The author will usually make a subdirectory in the galaxy's folder called “old” or “try1” and move all the files there for safe keeping, expect for the raw data. Then restart the pipeline as normal. It will lead you to the fiber ID step again. This time, enter `no` when it asks to find apertures automatically. Now, you will be able to manually mark the apertures, using `m` to mark and `d` to delete if necessary. It's important to make sure no apertures are marked twice, and that they go in order from 1 to 750 or 1500 from left to right.

For the second issue, if you know which fiber you need to turn off in the MDF, you can edit it manually and then restart the pipeline as detailed in the previous paragraph. To mark a fiber as bad, you can read in the appropriate fits file in IDL or Python, and change the BEAM entry for the fiber(s) of your choice. In Python, this process will probably look something like this (for the example of marking fiber 745 as bad):

```
>>> from astropy.io import fits
>>> import numpy as np
>>> hdulist = fits.open('gsifu_slits_mdf.fits')
>>> table = hdulist[1].data
>>> table
FITS_rec(
[(1, 0.34640503, 4.8000002, 'I_1', 1, 49, 57),
 (2, 0.34640503, 4.5999999, 'I_2', 1, 47, 57),
 (3, 0.34640503, 4.4000001, 'I_3', 1, 45, 57), ...,
 (1498, 3.117645, 4.4000001, 'A_3', 1, 45, 41),
 (1499, 3.117645, 4.5999999, 'A_2', 1, 47, 41),
 (1500, 3.117645, 4.8000002, 'A_1', -1, 49, 41)],
dtype=[('NO', '>i4'), ('XINST', '>f4'), ('YINST', '>f4'), ('BLOCK', 'S5'),
       ('BEAM', '>i4'), ('XLDIS', '>i4'), ('YLDIS', '>i4')])
>>> sel = np.where(table['NO'] == 745)[0][0]
>>> sel
744
>>> table['BEAM'][sel] = -1
>>> hdulist.writeto('newMDF.fits')
```

Once created, you can feed the edited MDF file to the pipeline code as one of your first steps of the reduction process.

### 4.3.2 A Bad Wavelength Solution

If something looks wrong, an easy way to fix this is to delete the ID files outside of the pipeline created in the previous step along with the “terg” files, and start again. If you're in 2-slit mode and see that only one of the slits is bad, you can delete only the bad one of these files (either “\_001” for the first slit and “\_002” for the second slit), and move the other one to a temporary file name. For example, if you find slit 2 is bad for one of the arcs, you can `rm` `IDergS...arc1_002`, and `mv` `IDergS...arc2_001` to a temporary file name. Now you can restart the pipeline, go to the wavelength calibration step, answer `NO` for slit 1 and redo the fits for slit 2. There will now be two new ID files, and you can replace `IDergS...arc1_001` with your temp file.

### 4.3.3 Correcting the 2014B Data with Bad Amplifier Effects

The blue setup RESOLVE data from the 2014B semester were heavily impacted by a bad column on the new CCDs installed on the telescope that summer. As detailed at [www.gemini.edu/node/10626](http://www.gemini.edu/node/10626)

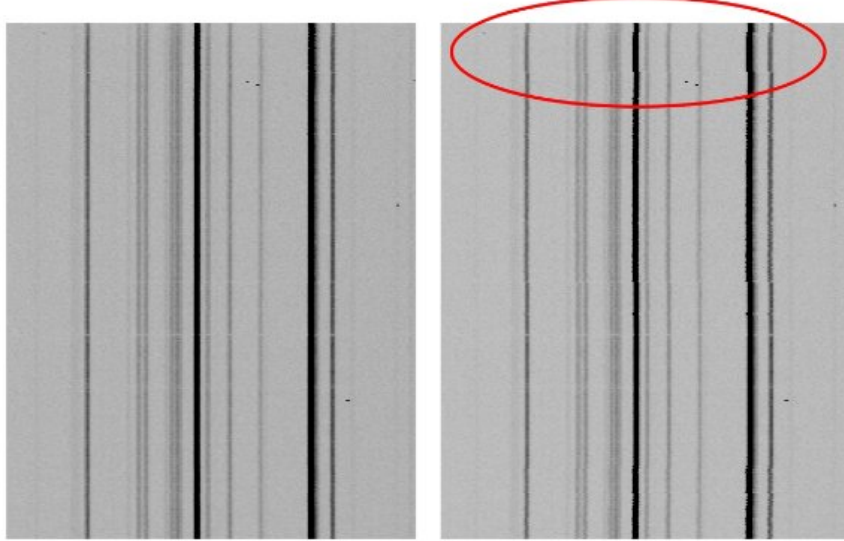


Figure 4.3: On the left is an image of a correctly transformed arc. On the right is an arc with a bad wavelength transformation. In particular, the circled red region shows how the emission lines are jagged in places. Image is Figure A.7 from <http://arxiv.org/abs/1409.8264>.

on February 26, 2015, the problem started as a bad pixel and has gradually gotten over the course of the semester. In [Figure 4.4](#), we show data taken early in the semester, when the hot pixel had spread only to a small part of the CCD read out through amplifier 5. In contrast, we show on the left side of [Figure 4.5](#) data taken late in the semester, where the issue is affecting the entire amplifier section. This only affected the blue setup seriously, since the exposure times in the blue setup are twice as long as those for the red setup (1200s vs. 600s each). This also means that the arcs and flats were not affected either.

Originally, the data was thought to be lost, until German Gimeno at the Gemini Observatory created a flat for us from data taken in 2013B. This flat is shown in [Figure 4.6](#). It is the same size as the effected amplifier region in [Figure 4.5](#), and when divided into the bad region, the saturation effects are removed.

The script to perform the correction and the flat file are both on cielo in the folder `/srv/two/emsnyder/gemini/data/2014B/scriptsfromgerman/`. The script is named `amp5improv_20160107.cl` and the flat is called `gout_5B.fits`. For data like in [Figure 4.5](#), where the bad regions span the full y direction, you can use this flat in full. For smaller regions of bad data, as in [Figure 4.4](#), you will need to copy the flat to a new file name and change the value of the regions not affected to one, so that dividing by the flat will leave those regions unchanged.

This cl script will not run properly in PyRAF, but works fine inside IRAF only. So, start IRAF, and move to the folder where your scripts are located. Then, copy over the science files you want to correct to this folder. I like working in a different folder from the rest of the data so that there's a copy of the original science files.

To perform correctly, the files need to have the MDF attached to them, i.e., have the prefix “g” before the file name. If you already have these created, copy them to this folder instead. If not, you can make them now. Inside IRAF, load the gemini and gmos packages by typing `gemini` and then `gmos`. Then use the task `gprepare` to add the MDF by typing: `gprepare filename fl_addmdf=yes`. If you have a special MDF, you can add `mdffile=filename` to the previous command. You should now have files with the prefix “g” to correct.

Next, make a txt file that just has the names of the files you want to correct listed, as so:

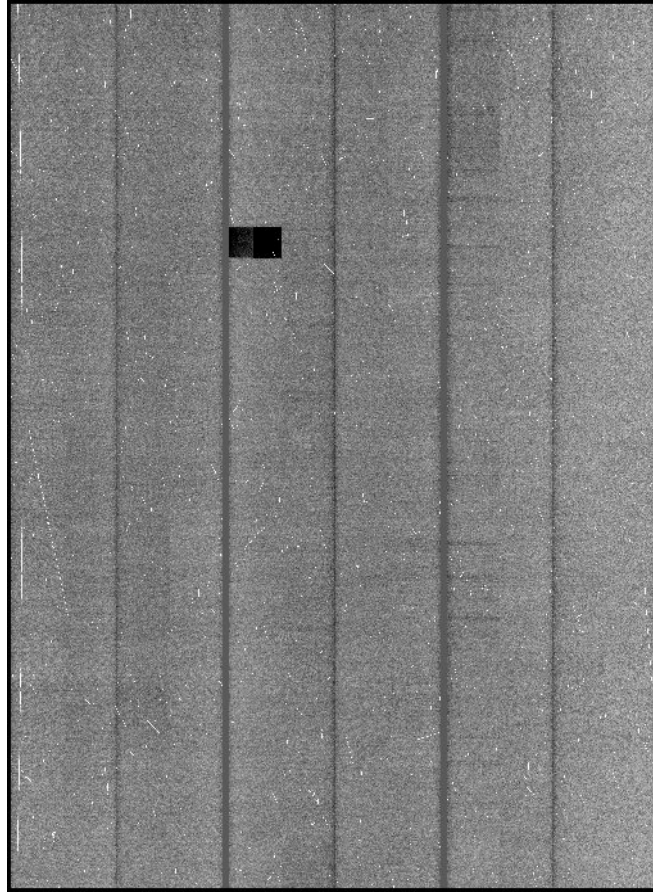


Figure 4.4

```
gS20141228S0030.fits  
gS20141228S0035.fits
```

The script looks in this text file to know which files to correct. Inside the script, you can also change the name of the flat file, if you created a new flat to span a smaller region. To run the script, inside IRAF type `c1 < amp5improv_20160107.cl`. The output files have the prefix “cg”.

Now to get back into the pipeline to complete the reduction, copy the “cg” files back to your galaxy folder. The pipeline will crash if there’s a file with the prefix “g” already, so you’ll need to complete the next step of the reduction before restarting the pipeline. This is the bias/overscan subtraction and image trimming step. Use the following command in IRAF to do this:

```
gfreduce filename outimag='rgS....' slits='red' or 'blue' fl_inter- fl_over+ fl_trim+ \  
fl_bias+ fl_flux- fl_gscrrej- fl_extrac- fl_gsappwave- fl_wavtran- fl_skysub- \  
weights- bias='biasfilename' mdffile='yourmdffile'
```

where filename will be your “cg” file (without .fits at the end!), outimage should be just “rg” so that the pipeline will know to use it, slits should be either red or blue depending on your setup, bias is the name of your bias frame, and mdffile is the MDF file (put default if you don’t have a special one made). This will make the “rg” file that will go on to be BPM corrected when you restart the pipeline.

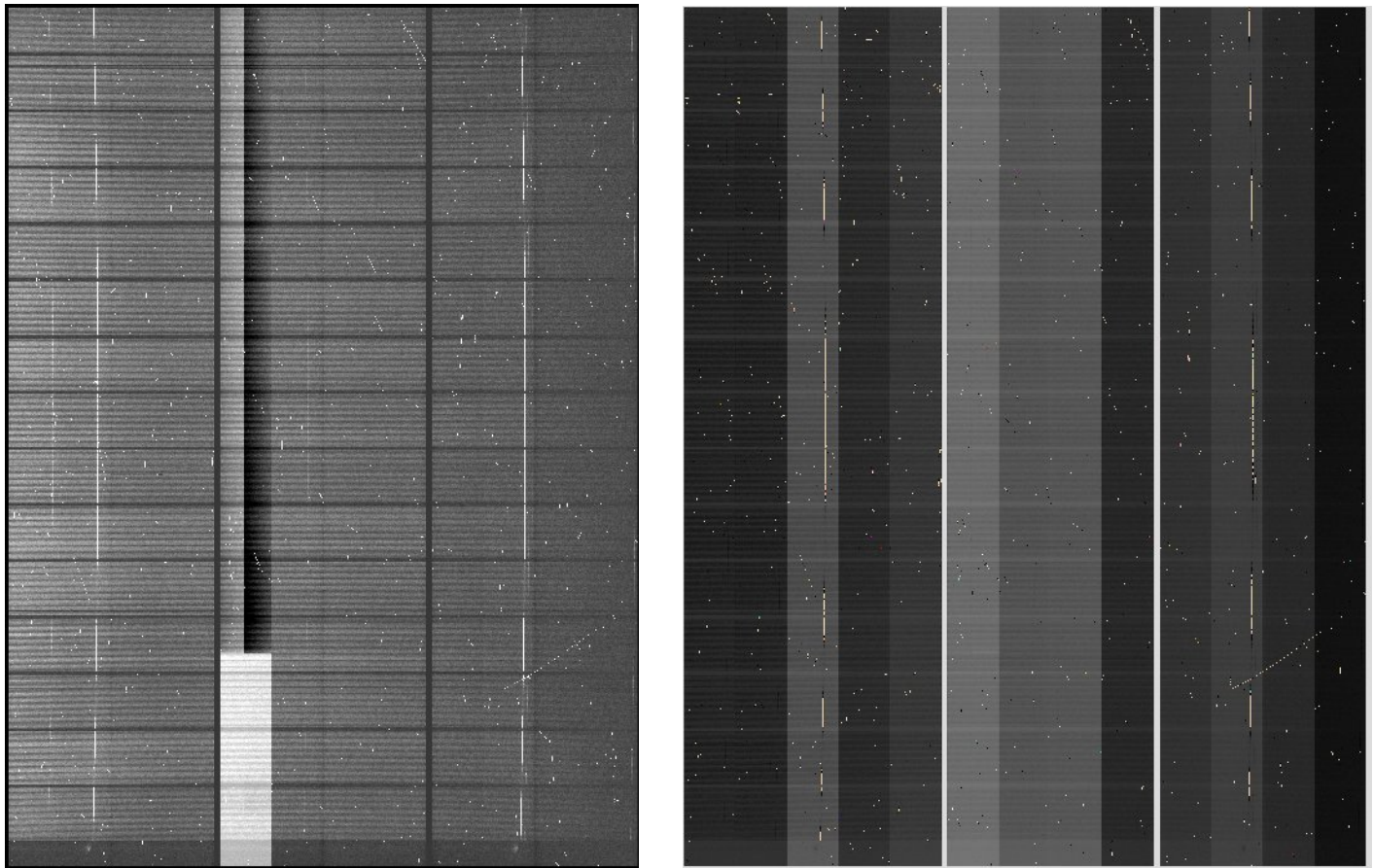


Figure 4.5: **(a).** Before and **(b).** after the amplifier 5 region in the data being corrected using the flat made by German Gimeno.



Figure 4.6: This is the flat created and given to us from German Gimeno. It is the width of one amplifier region, and spans the full y direction of the CCD.

